INTERANNUAL VARIABILITY OF WIND POWER INPUT TO NEAR-INERTIAL CURRENTS IN THE NORTH ATLANTIC

Tina Dippe
903123

Master Thesis to complete the M.Sc. program "Climate Physics" at the
GEOMAR Helmholtz Centre for Ocean Research, Kiel,
Christian-Albrechts-Universität zu Kiel

First Reviewer:	Prof. Dr. rer. nat. Richard Greatbatch
Second Reviewer:	Dr. rer. nat. Marcus Dengler

Abstract

Near-inertial oscillations are an important feature of the climate system. The output of a high-resolution ocean model of the North Atlantic was used to investigate interannual variability of wind power input (WPI) to near-inertial currents with respect to the North Atlantic Oscillation (NAO). The model is forced with NCEP/NCAR reanalysis wind stress for JFM of the years 1989 (strong positive NAO-phase) and 2010 (negative NAO).

Atmospheric parameters are tightly related to the NAO. The storm track in 1989 is intensified and channels storms into the subpolar North Atlantic, while it is more fanned out in 2010, allowing single storms to travel into the Mediterranean Sea. Similar patterns emerge from the distribution of near-inertial wind stress magnitude (NIWSM), i.e. the part of the wind stress spectrum that is most efficient in generating near-inertial energy (NIE). Seasonally averaged NIWSM, however, is not anchored to the storm track but is shifted to the south. This behaviour is due to the latitude-dependent inertial frequency, which decouples synoptic variability from the near-inertial frequency band.

WPI for the two considered years is consistent with the different distributions of storms: While 1989 produced a total rate of WPI of 6.48 x 10^9 W (= GW) and a secondary centre of weakly increased WPI in the eastern subpolar North Atlantic corresponding to the intensified storm track in this region, total WPI in 2010 amounted to 9.64 GW and was associated with a strongly enhanced secondary centre of WPI in the subtropics. Although anomalies both in the storm track and mean NIWSM are more pronounced in the subpolar ocean basin, WPI prefers the subtropics. It is proposed that a mixture of atmospheric and oceanic processes is responsible for this asymmetry, chief among them the variation of the Coriolis frequency with latitude.

Patterns of WPI, mixed layer NIE, and NIE in the deep ocean are similar to each other. NIE decreases drastically with depth.

Mean NIWSM is a promising atmospheric proxy to WPI. Linear statistical models of WPI built from this quantity allow the estimation of total WPI for each winter (JFM) from 1980 to 2013 in low, mid-, and high-latitudes. Total WPI as well as mid-latitude WPI is only weakly correlated with the NAO. Low- and high-latitude WPI on the other hand is strongly correlated with the NAO, with the magnitude of correlation coefficients exceeding values of 0.8, suggesting that the relationship of WPI to the NAO lies in shifting the patterns of WPI. During negative NAO phases, WPI is pulled towards the subtropics (and thus intensified), whereas it shifts towards the polar ocean during positive NAO phases, both in accordance with changes in the configuration of the storm track tail. Since the response of WPI to comparable mean NIWSM is weakening with latitude, total WPI is more strongly influenced by low-latitude WPI. It is concluded that the relationship between WPI in the North Atlantic and the NAO is of a twofold nature: While total WPI is only weakly and inversely related to the NAO, the distribution of WPI is strongly depending on it.

1.) Introduction

1.1) Near-inertial Energy

Near-inertial oscillations are an important feature of the climate system. In the surface mixed layer increased shear due to inertial oscillations provides a source of mixing that is capable of influencing SST patterns and thus the entire climate system (Jochum et al., 2013). The kinetic energy associated with near-inertial oscillations – referred to as near-inertial energy (NIE) throughout this thesis – is, however, not confined to the mixed layer, but can spread into the deep ocean in the form of near-inertial waves. Ground-breaking work on the dynamics and propagation of near-inertial waves has been carried out by Anderson and Gill (1979), Gill (1984) and Kunze (1985).

According to Munk and Wunsch (1998), an important role in maintaining the Meridional Overturning Circulation (MOC) against stratification may be played by energy that is fed to surface ocean currents by wind stress and leaks into the interior ocean in the form of dissipating internal waves subsequently. In their study, they estimated that a total of 2.1 TW is necessary to support the MOC. Roughly half of this amount possibly originates from wind forcing.

In the aftermath, a number of studies estimated the energy that is provided to inertial oscillations by wind power input (WPI) (e.g. Watanabe and Hibiya, 2002; Alford, 2003). While wind power input generally refers to kinetic energy that is transferred from the atmosphere to the ocean, WPI to inertial oscillations – or, equivalently, near-inertial currents – exclusively considers input to surface near-inertial energy. Low-frequency WPI to the general ocean circulation has been feasibly estimated (e.g. Oort et al., 1994; Wunsch, 1998). WPI to inertial oscillations, however, an important component of the total wind-work provided to the ocean, requires high temporal and spatial resolution of both the atmospheric and oceanic datasets employed. Since global datasets that would be fit for such a task have not been available in the past – and are, as of today, hard to acquire – investigations concerned with NIE have long been employing the slab model proposed by Pollard and Millard (1970). This model estimates the strength of near-inertial currents from wind stress and thus does not require an underlying dataset of oceanic surface currents.

Watanabe and Hibiya (2002) used the model to estimate global WPI to NIE and found a rate of 0.7 TW. Alford (2003) corrected this value to 0.47 TW, arguing that the slab model version employed by Watanabe and Hibiya (2002) did not incorporate polar regions realistically. Further revisions to this estimate will most likely be necessary. A recent study by Rath et al. (2013) for example found a reduction of up to 50% in WPI in the Southern Ocean when the ocean-surface-velocity dependence of the wind stress is accounted for. This finding suggests that previous estimates of WPI to near-inertial currents are (possibly: much) smaller than expected. On another note, a number of studies investigated how much NIE actually leaks into the deep ocean after being generated in the mixed layer. Both Furuichi et al. (2008) and Zhai et al. (2009) found that strong dissipation of NIE is taking place in the upper 200 m of the water column. According to these studies, a mere 15 to 25% of NIE escapes the upper ocean, providing at most 0.1 TW to deep-ocean mixing. The importance of NIE-triggered mixing for sustaining the MOC against stratification might have been overemphasized.

Another problem concerning WPI originates from the wind reanalysis products that are usually employed for climate studies. Gill (1984) and D'Asaro (1985) noted that it is mainly short-term fluctuations in the wind field that are most efficient in triggering WPI. However, the wind datasets commonly used for climate studies rarely have sampling periods shorter than six hours, implying that abrupt changes in the wind field are not sufficiently resolved. It

is possible that WPI in these studies is under-estimated. Beyond that, sufficient data coverage of the polar regions has long been an issue, and datasets are considered trustworthy only beginning in the 1980s, after the advent of satellite observations.

Yet another issue is discussed by Plueddemann and Farrar (2006). They highlight deficiencies of Pollard and Millard's (1970) slab model and advise to use more sophisticated, physically realistic models to approximate real-world mixed layer phenomena in modelling studies.

Simulating near-inertial currents in the mixed layer remains a challenging task.

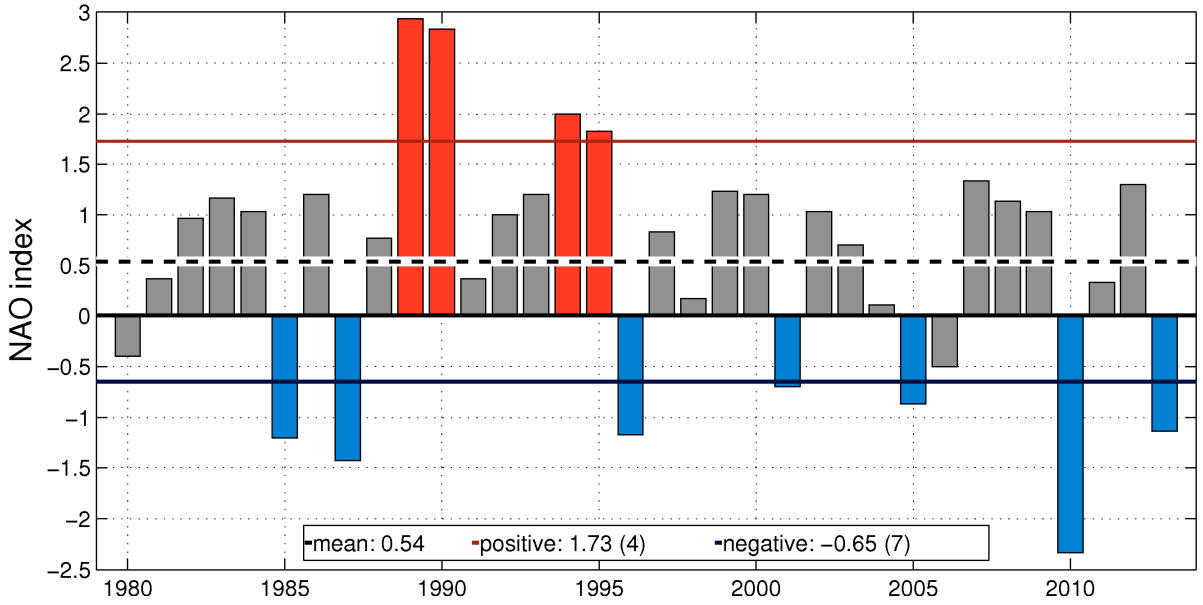

Figure 1: Hurrell's station-based NAO-index for the time span considered in this thesis (1980 – 2013), winter-average (JFM). Red (blue) bars denote the years that were used for composites of positive (negative) NAO conditions throughout this thesis. The dashed line shows the average NAO index for the considered time span (0.54). Composite averages are 2.40 and -1.26 for positive and negative conditions, respectively. Solid lines denote the mean of the time series ± one standard deviation (= criterion to be included in the composite).

1.2.) Interannual Variability: Scope of the Thesis and Atmospheric Variability

Studies of WPI have not yet investigated spatial and temporal variability of WPI. This thesis attempts to fill in some of the blanks in this field of research. The investigated area is the North Atlantic.

The North Atlantic plays an important role in internal climate variability, both in the atmospheric and oceanic component of the climate system (Marshall et al., 2001). The dominant mode of internal atmospheric variability in the North Atlantic sector is the North Atlantic Oscillation (NAO) (Hurrell, 1995). It essentially mirrors fluctuations in the relative configurations of the Icelandic Low and the Azores High. An index commonly used to describe the state of the NAO is the difference between normalized sea level pressure (SLP) at Lisbon, Portugal, and Stykkisholmur in the vicinity of Reykjavik, Iceland. Another measure is the time series associated with the first empirical orthogonal function of SLP in the North Atlantic (Hurrell et al., 2001). Figure 1 shows the station-based index of the NAO for the time span considered in this thesis.

The NAO is related to both interannual and decadal variability of North Atlantic winter climate (e.g. Greatbatch, 2000). Positive phases of the NAO are usually accompanied by mild and wet conditions in western Europe and cold, dry conditions in north-eastern North America and Greenland. Negative NAO conditions reverse this pattern. The mechanism steering these changes is connected to the variability of the North Atlantic storm track (see Ulbrich et al. (2009) for a review of current knowledge about the North Atlantic storm track): Positive NAO years tend to produce more intense and more frequent storms and shift the storm track into the Norwegian Sea. During negative NAO years, storms occur less frequently and are of reduced intensity. The storm track is more zonally oriented and allows more storms to enter the Mediterranean basin (Lau, 1988; Rogers, 1997). Several studies commented on the pronounced co-variability between the NAO and the North Atlantic storm track and suggested that it is not so much the NAO steering the North Atlantic storm track but rather the variability of the storm track and the associated changes in the SLP patterns that maintain the NAO (e.g. Benedict et al., 2004; Löptien and Ruprecht, 2005).

This thesis establishes a relationship between the interannual variability of wind power input to near-inertial currents and the NAO, based on the idea that the NAO can serve as a good indicator of storminess – i.e. of the spatial characteristics and intensity of the storm track – over the North Atlantic. We use output from a high-resolution primitive equation ocean model of the North Atlantic to investigate the response of the ocean to wind stress forcing taken from the winters exhibiting extremely high and low NAO indices (1989 and 2010, respectively). Section 2 reviews the employed model and the datasets used for evaluating atmospheric conditions with respect to the NAO-phase. Section 3 investigates the variability of both the storm track and near-inertial wind stress magnitude (NIWSM) in relation to the NAO. Section 4 presents the results of the ocean model runs, addressing both WPI and the distribution of NIE in the deep ocean. Section 5 identifies an adequate atmospheric proxy for WPI. Section 6 provides a summary and discussion of the findings as well as an outlook on future work.

2.) Model and Methods

2.1.) Near-inertial Quantities

To obtain near-inertial quantities, it is necessary to band-pass filter datasets. Filtering in this thesis was achieved by applying a 9th-order Butterworth-filter to the respective dataset. The near-inertial band is defined analogous to Rath et al. (2013): The band is centred at the local inertial frequency (= Coriolis frequency = $2\omega \sin(\varphi)$, where φ is the latitude). Upper and lower thresholds of the band for ocean currents and wind stress data are given by the Coriolis frequency at latitude $\varphi \pm 10°$N and $\varphi \pm 1°$N, respectively. The broader near-inertial band for ocean currents is justified, since the inertial peak in ocean current data is very pronounced. In contrast, wind variability displays no clear near-inertial peak. Thomson (1983) for example presents spectra for wind stress and points out that no inertial peak is evident.

Based on the filtered time series for the horizontal components of the wind stress, near inertial wind stress magnitude (NIWSM) is defined as

$$NIWSM(t) = \sqrt{\tau(t)_{x,I}^2 + \tau(t)_{y,I}^2} \ ,$$

where $\tau_{x,I}$ and $\tau_{y,I}$ are the near-inertial components of zonal and meridional wind stress, respectively. NIWSM is available for each time step t of the filtered time series. Mean NIWSM is the average of a NIWSM-time series at a given location.

Wind Power Input is calculated as

$$WPI = \vec{\tau} \cdot \vec{u}_{S,I} \ .$$

$\boldsymbol{\tau}$ is unfiltered wind stress, $\mathbf{u}_{S,I} = (u_I, v_I)$ is the surface velocity, where the horizontal components (u: zonal, v: meridional) have been filtered to retain frequencies in the near-inertial band. Wind stress for the calculation of WPI was obtained from the model. Although the model-wind stress technically is the same as NCEP/NCAR-wind stress (cf. section 2.2) albeit interpolated to a finer spatial and timely resolution, the interpolating procedure may have resulted in slight differences between the two wind stress datasets.

For analysing storm tracks (cf. section 3.1), SLP was filtered in the synoptic 2-6 days band (Ulbrich et al., 2009).

Composites in this study are based on the NAO index shown in Figure 1. Single years were included in the composite, if the NAO-index of that year departed from the mean NAO index by more than one standard deviation, based on the time span 1980 to 2013. Years contributing to the composite for positive NAO conditions are marked red in Figure 1, contributions to the negative NAO composite are marked blue.

2.2.) Atmospheric Datasets and Storm Track Measures

To investigate the atmospheric conditions associated with different NAO phases, we used the NCEP/NCAR reanalysis-dataset (Kalnay et al., 1996). Two components of the dataset provided data for this thesis: The "*surface flux*" section of the dataset contains zonal and horizontal momentum fluxes, which are identical with wind stress. Wind stress is provided on a Gaussian T62-grid every 6 hours. The "*surface*" section of the NCEP/NCAR-reanalysis dataset provides SLP data. Space and time resolution of the surface data is 2.5°lon x 2.5°lat and 6 hours, respectively.

Due to sparse data north of 70°N, analysis of NCEP/NCAR data – i.e.: data associated with the atmosphere – in this study is restricted to the North Atlantic domain between 20°N and 65°N. The datasets were obtained from NOAA's ESRL Physical Science Division (http://www.esrl.noaa.gov/psd/data/gridded/data.ncep.reanalysis.html). The NAO index was obtained from James Hurrell's web-site (https://climatedataguide.ucar.edu/climate-data/hurrell-north-atlantic-oscillation-nao-index-station-based).

Storm tracks were diagnosed in two ways: An average quantity was obtained by band-filtering SLP in the synoptic band and calculating its variance. This corresponds to the standard definition of a storm track (Ulbrich et al., 2009) and is referred to as storm *track* throughout this analysis. Additionally, actual storm path data was used to get an impression of what the individual winter storms in the years 1989 and 2010 looked like. The storm path data was provided by Sergey Gulev and Natalia Tilinina of the P. P. Shirshov Institute of Oceanology of the Russian Academy of Sciences. Gulev and Tilinina used the NCEP/NCAR dataset to diagnose the tracks of individual storm centres for the northern hemisphere by applying a semi-manual tracking algorithm (Gulev et al., 2001). To avoid confusion, individual storm centre tracks are referred to as storm *paths*.

2.3.) The Ocean Model

The ocean model is a version of the MIT General Circulation Model. Horizontal resolution is 1/10°, vertical resolution is variable, ranging from 10 m at the surface to 250 m at the ocean bottom with a total of 33 geopotential levels. Output is provided every 2.5 hours. The analysis region covers 14°S to 74°N and 100°W to 20°E. For further details, see Zhai and Marshall (2012).

The model was spun up for a total of 53 years with climatological monthly mean forcing obtained from the NCEP/NCAR reanalysis. Horizontal resolution during the first 23 years of the spin-up was 1/5°. For the remaining 30 years, the full resolution of 1/10° was applied. Both model runs were initialized with the end of the spin-up, corresponding to Dec 31 24:00:00. Wind stress forcing for the experiments is taken from the NCEP/NCAR reanalysis for the winters of 1989 and 2010 (JFM). The NAO during these two years was extreme. The NAO index for 1989 is the most positive since the advent of satellite observations (2.93), and it is most negative for 2010 (-2.33).

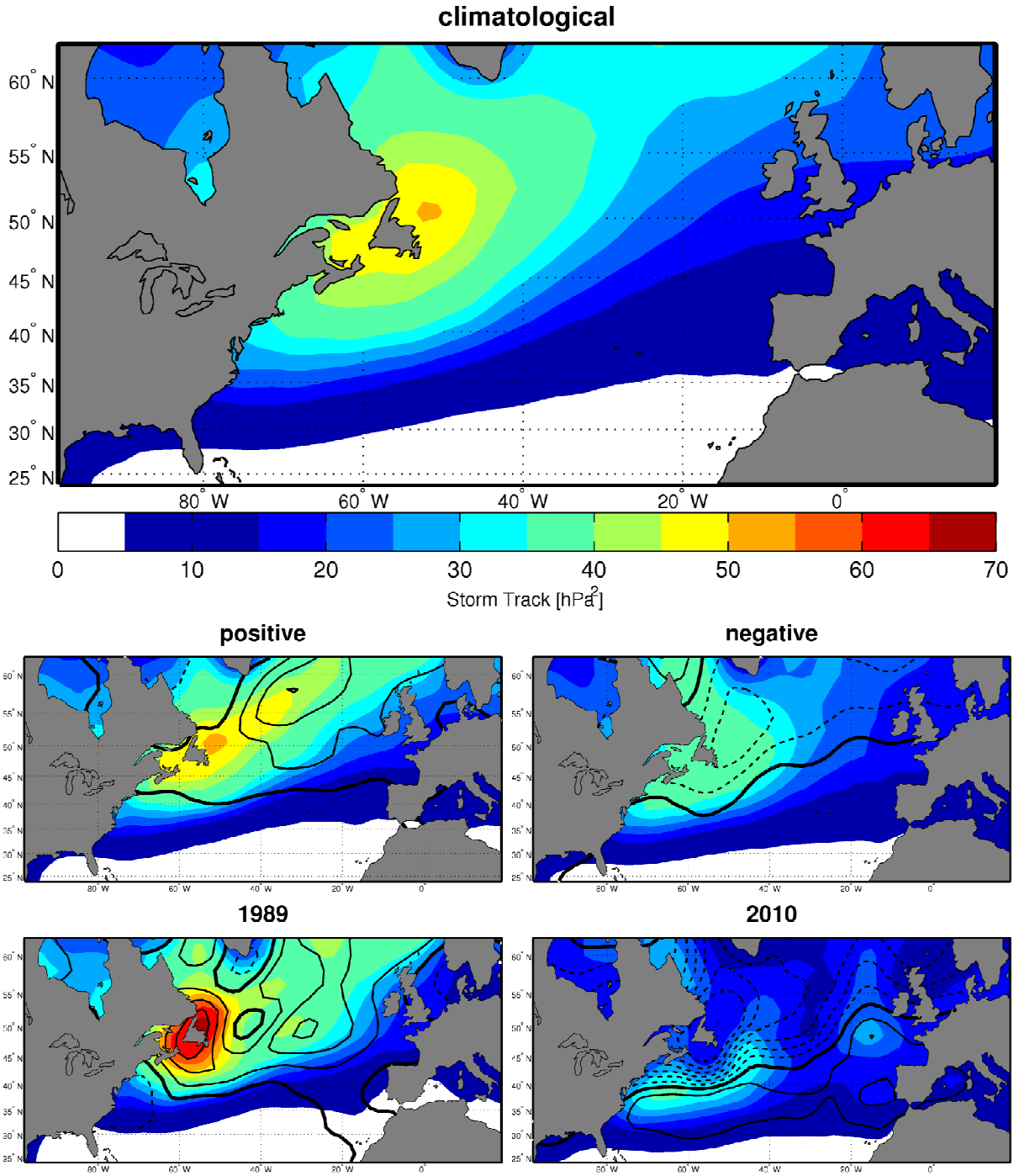

Figure 2: Storm Track (synoptic SLP variance). Top: climatological (1980 – 2013; the storm track has been calculated for each winter season (JFM), subsequent averaging yielded the mean and composite patterns). Middle panels: composite storm tracks for positive NAO conditions (left) and negative NAO conditions (right). Bottom panels: single-year storm tracks for 1989 (left) and 2010 (right). Black contour lines denote storm track anomalies. Solid (dashed) lines indicate positive (negative) anomalies, with the thick black line being associated with 0. The contour interval is 5 hPa^2.

3.) The Dependence of Atmospheric Conditions on the NAO Phase

3.1.) The North Atlantic Storm Track

The North Atlantic storm track is a key feature of the North Atlantic winter climate. Figure 2 (top) shows the climatological winter storm track in the North Atlantic. It is obtained by band-pass filtering SLP to retain variability in the synoptic 2-6 days band for the period 1980 to 2013. Subsequent calculation of variance for each cold season (JFM) and averaging of this quantity yields the climatological storm track. Note that the chosen approach does not only reflect SLP variability due to cyclones but also includes anticyclones. Thus, this kind of storm track has sometimes been referred to as the "synoptic wave-guide". (Lau, 1988)

The NCEP/NCAR-SLP based storm track compares well with other studies (e.g. Ulbrich et al., 2009). Enhanced synoptic variability is centred over Newfoundland. This region is referred to throughout the thesis as "*core storm track*". The "*storm track tail*" is the extension of the core storm track into the eastern North Atlantic. For the climatology, it stretches northeastward towards the Nordic Seas. Relatively little synoptic variability is found in the subtropical eastern North Atlantic.

Composite storm tracks for positive and negative NAO conditions are shown in Figure 2 (middle panels, absolute storm track in shading, anomalies as contour lines). During positive NAO years, the storm track in the north-eastern North Atlantic is intensified by magnitudes of up to 10 hPa^2, suggesting a shift of the storm track tail from its climatological position into the Nordic Seas. The core storm track is weakly intensified. Intensification in general takes place north of 45°N with the exception of the Labrador Sea. It is strongest southwest of Iceland. Decreases in storm track intensity in the subtropical North Atlantic do not fall below values of -5 hPa^2.

During negative NAO years, the storm track pattern is reversed. The entire storm track is markedly weakened relative to the climatology. Anomalies are negative throughout the North Atlantic north of 45°N, and weakly positive in the subtropical North Atlantic and the Labrador Sea. The strongest decrease of -10 hPa^2 occurs in the core storm track. In the subtropical North Atlantic, synoptic SLP variability increases, although the anomalies do not exceed 5 hPa^2 in the composite. The centre of positive anomalies is located at roughly 40°N, 40°W and is elongated westwards towards Portugal (not shown). A weak secondary centre of 4 hPa^2 is situated directly off the Portuguese coast. Positive anomalies in the Labrador Sea are bigger than 5 hPa^2. This pattern suggests a general weakening and more zonal orientation of the storm track, shifting its tail into the Gulf of Biscay and the Mediterranean basin and the whole storm track towards the tropics.

Overall, the NAO shows strong co-variability with two characteristics of the North Atlantic storm track: Both the intensity of the storm track and the position of the storm track tail show a pronounced relationship with the NAO. These findings agree well with former studies on the subject (Greatbatch, 2000; Rogers, 1997).

To illustrate the storm track configurations of 1989 and 2010, Figure 3 shows the individual storm paths of these winters. It is consistent with what has been found in the composite analysis. In 1989, storm paths are concentrated along an axis tilted in a southwest-northeasterly fashion stretching from Cape Hatteras towards the Nordic Seas. Intense systems occur more frequently than usual. A total of 223 storms were counted in the North Atlantic sector, with the mean minimum core pressure of the systems being 986 hPa. In terms of the standard storm track, the composite pattern for positive NAO-conditions is increased for 1989

in the core storm track region (Figure 2, bottom): While synoptic SLP variance in the north-eastern North Atlantic exceeds the climatological storm track by about 10 hPa^2 (note, however, that the strongest anomalies are displaced slightly to the north-east relative to the secondary centre of increased SLP variability of the composite pattern), anomalies in the core storm track region reach values of more than 15 hPa^2 and are not shifted to the west. The core storm track is strongly enhanced in the winter of 1989, with its tail being notably shifted into the Nordic Seas.

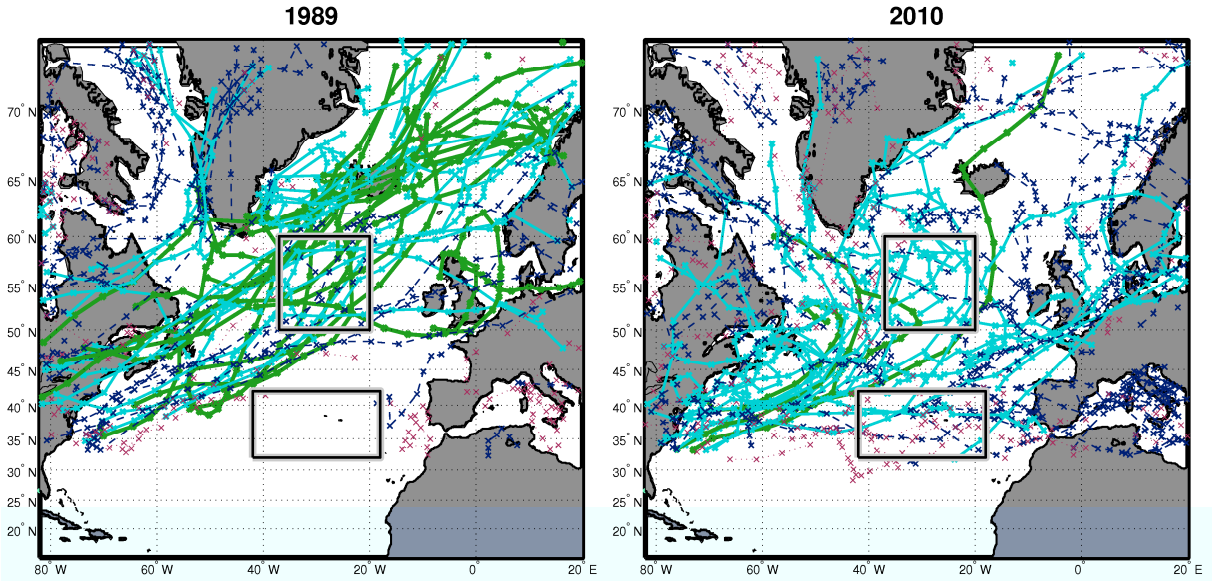

Figure 3: Winter storm paths (JFM), 1989 (left) and 2010 (right). The line style of a storm path corresponds to the maximum intensity of the system in terms of minimum core pressure. Green: < 960 hPa, light blue: < 980 hPa, dark blue: < 1000 hPa, mauve: > 1000 hPa. Black boxes denote the region of enhanced WPI in the subpolar (subtropical) North Atlantic in 1989 (2010), cf. Figure 8.

In comparison, Figure 3 (right) shows the winter storm paths for 2010. Individual storm paths are less clustered with a number of storms travelling in a rather zonal fashion, penetrating the eastern North Atlantic as far south as 35°N. Occurrences in the Mediterranean basin increase, as does the frequency of storms reaching the southern European coast. The number of storms travelling into the north-eastern North Atlantic is greatly reduced. The distribution of minimum core pressures is slimmed relative to the distribution for 1989 (not shown): Intense systems occur less frequently, the mean maximum intensity in units of core pressure is 991 hPa. A total of 219 storms occurred. The standard storm track (Figure 2, bottom) is displaced to the south by roughly 10°. Pronounced deviations of more than -30 hPa^2 occur in the core storm track region, while positive anomalies with magnitudes of roughly 10 hPa^2 are found south of the climatological storm track and west of Europe, notably in the Gulf of Biscay and off the Portuguese coast. This pattern suggests a general decrease in weather system intensity during the winter of 2010 and a pronounced southward shift and more zonal orientation of the storm track tail.

Overall, the winters of 1989 and 2010 agree well with the composites for negative and positive NAO years discussed earlier. Patterns of deviations from climatological conditions are enhanced relative to the composite patterns. Individual storm paths mirror the storm track.

According to Gill (1984) and D'Asaro (1985), it is frontal structures and small translating lows that trigger efficient generation of inertial oscillations in the surface mixed layer. As these features are usually incorporated in synoptic-scale extratropical storms, we expect the two sets of storm distributions to have different impacts on WPI.

3.2.) Storm Track Variability and near-inertial Components of Wind Stress

Near-inertial wind stress magnitude (NIWSM) represents the strength of the wind stress in the near-inertial band, i.e. the part of wind stress variability that is most efficient in creating near-inertial currents (Rath, 2013). It is appropriate to assume that NIWSM is intimately related to the generation of inertial oscillations and thus to WPI. This section investigates the relationship of mean NIWSM with the NAO.

Due to the squaring of the wind stress components, NIWSM values for any location have a gamma-like distribution, with low values providing the bulk of samples and a few high values influencing the arithmetic mean rather strongly. Consequently, high mean NIWSM values may reflect strong intermittent events rather than continuously enhanced NIWSM throughout the entire season. Variance remains a measure of average spreading from the mean, but is of little practical interest for this study. Skewness and kurtosis in general describe the shape of a distribution differing from the Gaussian distribution. They are related to the third and fourth central statistical moments, respectively, and emphasize strong deviations from the mean. Skewness gives an impression of how strongly a distribution leans towards values that correspond to positive or negative deviations from the mean. Kurtosis is regarded as a measure of "peakiness" of the distribution and has been used to assess the intermittency of events contributing strongly to the mean (e.g. D'Asaro, 1985). Here, skewness is a measure of the shape parameter of a gamma-distribution, i.e. describing how fast the probability density function decays towards zero. The faster the decay, the more positive the skewness is expected to be. High skewness of a NIWSM time series indicates a location that is struck by strong NIWSM events only rarely. This corresponds to kurtosis: high values of kurtosis arise if peaks in the NIWSM time series occur infrequently. Both of these quantities thus help to identify regions in which strong NIWSM events are scarce. Because kurtosis is the traditional measure of intermittency, we restrict our analysis of statistical properties of NIWSM to mean NIWSM and kurtosis and omit skewness. Indeed, inspecting patterns of NIWSM-skewness and kurtosis reveals that they are virtually indistinguishable from each other (not shown).

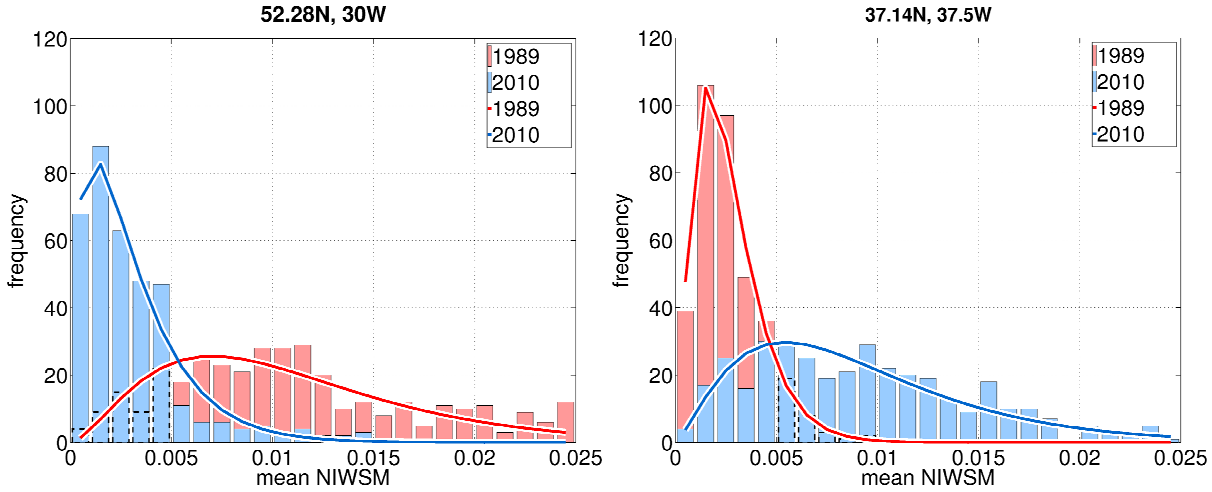

Figure 4: Sample histograms of NIWSM from NCEP/NCAR for JFM, and fitted gamma-distribution for the subpolar ocean (54.28°N, 30°W, left) and the subtropical ocean (37.14°N, 37.5°W, right). Sample locations were chosen to coincide with maximum mean NIWSM (cf. Figure 6) in the subpolar ocean in 1989 and in the subtropics in 2010. Mean NIWSM values were 0.011 and 0.009 Nm^{-2} in the subpolar ocean in 1989 and the subtropics in 2010, respectively. Light Red (light blue) bars denote the raw histogram in 1989 (2010). Note that the 2010 histogram is in the foreground. When the frequency of mean NIWSM in a given bin is lower in 1989 than in 2010, the 1989 frequencies are denoted by dashed black bars. The fitted gamma-distribution is denoted by solid lines (red for 1989, blue for 2010).

Figure 4 shows examples of the distribution of mean NIWSM in the subtropical and subpolar North Atlantic. Both the actual histogram of NIWSM and a fitted gamma-distribution are shown to illustrate the meaning of the statistical quantities discussed above. The histogram of mean NIWSM in the subpolar ocean basin leans heavily towards small values in 2010 and is notably shifted towards higher values in 1989, suggesting that mean NIWSM in 1989 is strongly increased relative to 2010. Indeed, mean NIWSM values were 0.011 and 0.003 in 1989 and 2010, respectively (based on the histogram). The shape and scale parameters of the fitted gamma-distribution were 2.73 (1.59) and 0.004 (0.002) in 1989 (2010), respectively. NIWSM kurtosis during JFM of 1989 and 2010 was 2.55 and 7.34, supporting the argument that NIWSM events in the 2010 subpolar North Atlantic were less frequent than in 1989 (cf. Figure 3). In the subtropical North Atlantic, the histograms are basically swapped for 1989 and 2010: The 1989 histogram is skewed towards small NIWSM values, mean NIWSM was 0.003 and 0.009 for 1989 and 2010, respectively. The shape and scale parameters of the fitted gamma-distribution were 2.62 (2.42) and 0.001 (0.004) in 1989 (2010). NIWSM kurtosis was 4.80 and 2.71 for 1989 and 2010, respectively.

The top panels of Figures 5 and 6 show the climatological patterns of mean NIWSM and NIWSM kurtosis as well as the climatological storm track based on the winters 1980 to 2013 (JFM). The storm track is shown as contour lines and corresponds to shading in the top panel of Figure 2. Values for the climatological NIWSM-quantities were obtained by calculating a single value for each winter (JFM) between 1980 and 2013 and subsequent averaging of these seasonal values. The middle panels of Figures 5 and 6 show composites of the same quantities. Contours in the middle and bottom panels denote the absolute storm track in Figure 5 and storm track anomalies in Figure 6 (positive anomalies are indicated by solid lines, negative anomalies by dashed lines). The unit of both storm track quantities is hPa^2.

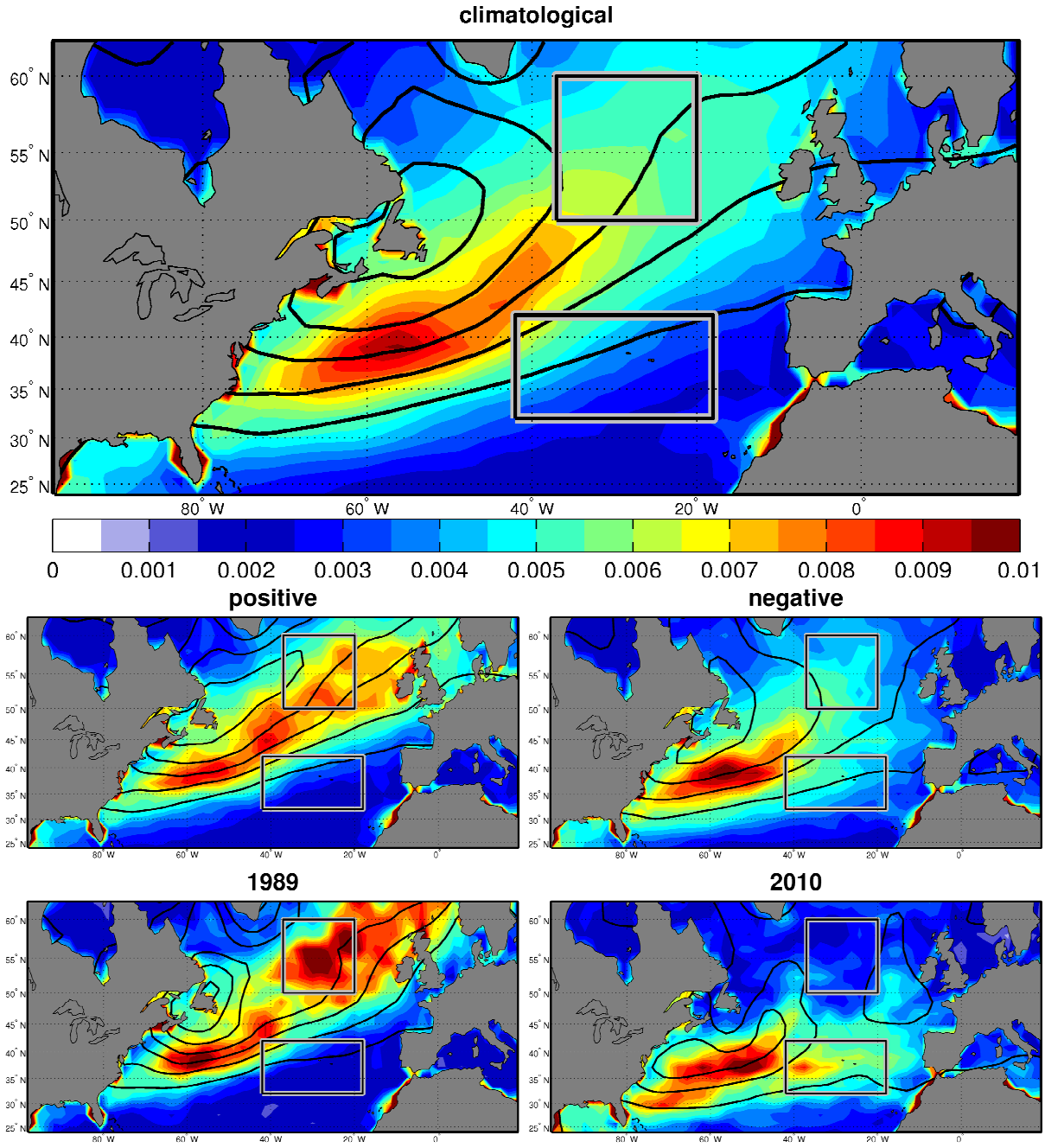

Figure 5: Mean NIWSM [Nm^{-2}] in JFM (shading) and storm track (black contour lines). Top: climatology (1980 – 2013), middle: NAO composites (right: positive, left: negative), bottom: 1989 (left) and 2010 (right). Shading is equal in all panels. The storm track contour interval is 10 hPa^2, first contour line is 10 hPa^2. Black boxes as in Figure 3.

The climatological pattern of mean NIWSM (top panel of Figure 5) displays high values that are arranged in an almond-shaped patch between 35 to 42°N, 70 to 40°W, stretching northeastward towards the UK. A weak secondary centre emerges at roughly 45°W, accompanying a slight northward tilt of the pattern. Maximum values are found to be roughly 10 x 10^{-3} Nm^{-2}. Note that the mean NIWSM pattern resembles the storm track in shape but is displaced approximately 10° to the south of it. A discussion of this counter-intuitive feature is provided in section 3.3.

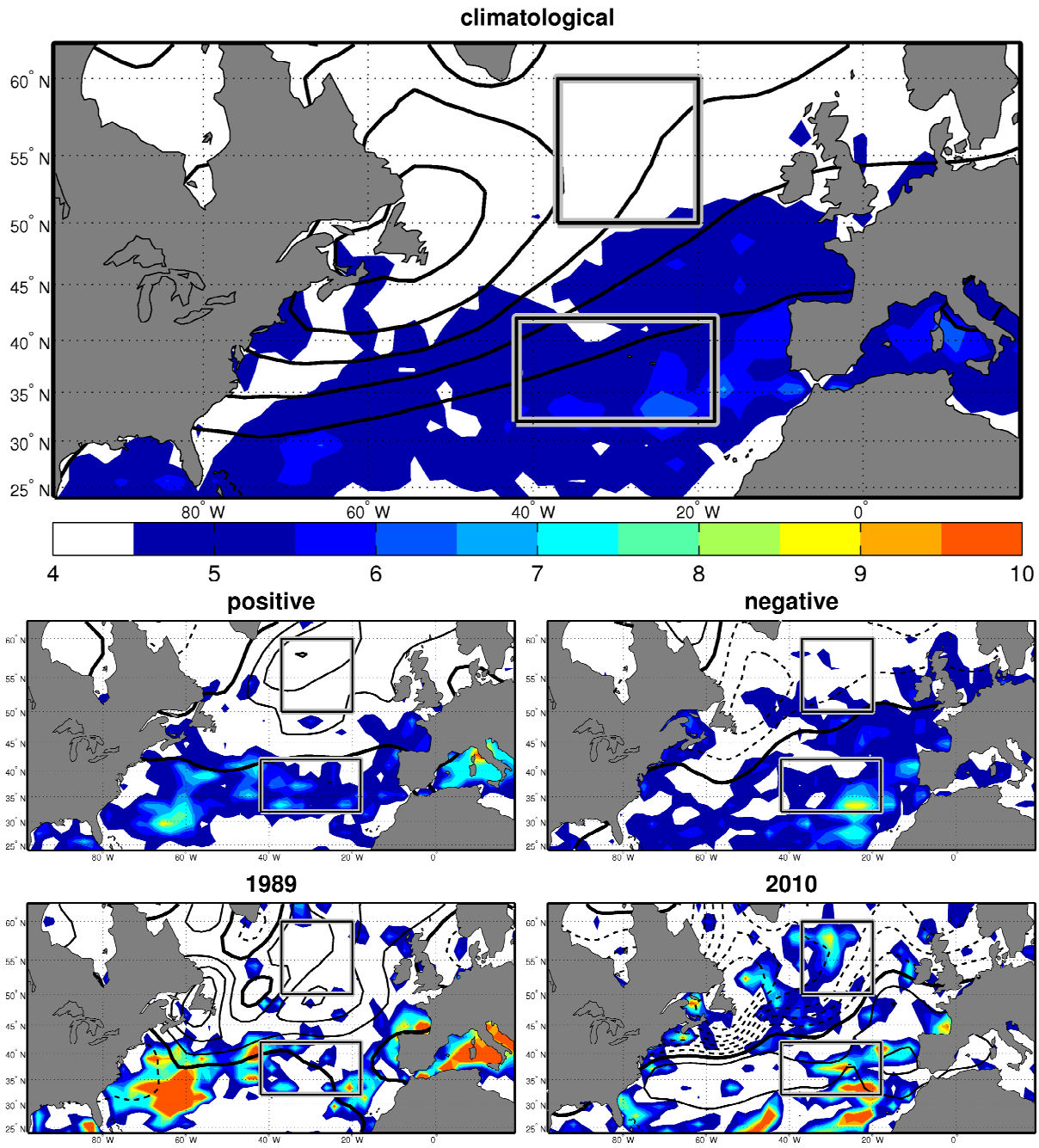

Figure 6: NIWSM kurtosis (shading). Top: climatology (1980 – 2013) and climatological storm track (black contours, 1980 – 2013). Middle and bottom: NIWSM kurtosis and storm track anomalies. Middle: positive NAO (left), negative NAO (right), bottom: 1989 (left), 2010 (right). Shading is equal in all panels. The contour interval for the climatological storm track is 10 hPa^2, the first contour line is 10 hPa^2. The contour interval for the storm track anomalies is 5 hPa^2. Positive and negative anomalies are denoted by solid and dashed contour lines, respectively. The thick solid contour line denotes 0. Black boxes as in Figure 3.

Composites of mean NIWSM are shown in the middle panels of Figure 5. For positive NAO phases, the location of enhanced mean NIWSM in the western subtropical North Atlantic appears only marginally changed relative to climatological conditions. Enhanced mean NIWSM in the mid- and subpolar latitudes is much more pronounced and reaches magnitudes of up 8.5 x 10^{-3} Nm^{-2}. It is oriented along an axis that is tilted in a southwest-northeastward-fashion. This coincides with the orientation of the storm track axis (shown as black contour lines). As for climatological conditions, the mean NIWSM pattern resembles the storm track pattern but is displaced approximately 10° to the south of it. Deviations from

the climatology (not shown) are barely perceptible in the western subtropical North Atlantic but reach magnitudes of 2 to 3 Nm^{-2} in the subpolar North Atlantic. In general, mean NIWSM anomalies for positive NAO conditions are positive in the north-eastern North Atlantic, with the strongest positive anomalies occurring to the west of the British Isles. Anomalies are weakly negative in the North Atlantic south of 45°N as well as in the Labrador Sea.

During negative NAO conditions, mean NIWSM in the western subtropical North Atlantic is weakly enhanced and reaches values of 10 x 10^{-3} Nm^{-2}. Mean NIWSM in the subtropical North Atlantic is generally increased, relative to both climatological conditions and positive NAO conditions (note how regions of very low mean NIWSM, shown as dark blue shading, are pushed more pronouncedly towards the equator). In the mid-latitudes and subtropical North Atlantic mean NIWSM is visibly decreased. This pattern is similar to the storm track pattern. The shift of mean NIWSM relative to the storm track is, again, present. Mean NIWSM anomalies (not shown) relative to the climatology are similar in magnitude and distribution to positive NAO conditions but are reversed in sign, indicating that mean NIWSM in the tropics is generally increased during negative NAO conditions and decreased during negative NAO conditions. The opposite is true for the subpolar North Atlantic.

Patterns of absolute mean NIWSM values for 1989 and 2010 (bottom panels of Figure 5) agree well with the composite pattern in shape. Their magnitude is increased relative to the composite patterns. In 1989, the subtropical North Atlantic is basically void of near-inertial wind stress, whereas strong positive values of up to 10 x 10^{-3} Nm^{-2} occur in the subpolar North Atlantic basin. In contrast, mean NIWSM in 2010 exhibits a more zonal pattern with a secondary centre of magnitude 8 x 10^{-3} Nm^{-2} occurring in the eastern subtropical North Atlantic. The mean NIWSM-equivalent of the core storm track appears unchanged in both years, albeit the 2010-patch is displaced by some 5° to the east. Anomalies relative to the climatology (not shown) agree in sign with the composite patterns, but reach magnitudes of up to twice the composite magnitudes in the eastern North Atlantic.

Climatological NIWSM kurtosis is shown in Figure 6 (top). Generally low values are found in the mid-latitudinal and northern North Atlantic. NIWSM kurtosis decreases steadily towards the pole, while a band of increased kurtosis values emerges in the subtropical North Atlantic, incorporating the Gulf of Biscay. Again, the boundary between enhanced and low kurtosis values is tilted in the southwest-northeasterly fashion associated with the storm track. The pattern supports little storm activity in the subtropical North Atlantic, consistent with the analysis of the SLP-based storm track.

NIWSM kurtosis composites in response to different NAO regimes are shown in Figure 6 (middle). Patterns of NIWSM kurtosis can be linked to storm track anomalies: During positive NAO conditions, NIWSM kurtosis is generally increased in the subtropical North Atlantic. This coincides with weak negative storm track anomalies, suggesting that strong NIWSM events occur less frequently in these regions, which, in turn, is consistent with storms occurring less frequently. Pronounced positive storm track anomalies in the subpolar North Atlantic on the other hand do not decrease NIWSM kurtosis notably, indicating that the frequency of storms relative to climatological conditions is only weakly affected by the NAO phase.

The NIWSM kurtosis pattern for negative NAO conditions is similar to positive NAO conditions at first sight, although storm track anomalies swap signs in the subtropical and subpolar North Atlantic. In the western subtropical North Atlantic, little deviation from climatological conditions is perceptible in the distribution of absolute NIWSM kurtosis. However, NIWSM kurtosis anomalies (not shown) are indeed weakly negative, which is consistent with increased storminess in this region. In the subpolar North Atlantic, no striking changes are present in NIWSM kurtosis for negative NAO conditions. NIWSM kurtosis

anomalies are distributed in a patchy pattern, implying that, albeit storms are growing less intense during negative NAO phases in the northern North Atlantic, their frequency is not notably reduced. Finally, in the eastern subtropical North Atlantic, NIWSM kurtosis is markedly increased, suggesting *less* frequent NIWSM events. This seems to be at odds with weakly positive storm track anomalies at first. An explanation for this behaviour is provided below.

Patterns of NIWSM-kurtosis for 1989 and 2010 (bottom panels of Figure 6) are not as readily comparable to composite conditions as for the mean NIWSM case. Notable responses can be found in both years in the subtropical North Atlantic and in the Mediterranean basin. In the subtropical western North Atlantic south of the core storm track between 40 and 20°N, the intermittency of high-NIWSM events is increased for 1989 and decreased for 2010, which is in accordance with a shift of the storm track towards the pole and the equator, respectively. NIWSM kurtosis in the Mediterranean basin is increased for 1989 and decreased in 2010, consistent with decreased and increased cyclone frequencies in the respective years. In regard of these arguments, the distribution of NIWSM kurtosis in the eastern subtropical North Atlantic – low in 1989 (indicating frequent strong NIWSM events), high in 2010 (infrequent strong NIWSM events) – might be confusing at first. However, Figure 3 confirms that no storm passes the subtropical eastern North Atlantic in 1989, while a number of systems travel through the region in 2010. Consider that the background wind regime in this region can be associated with the transition zone between the trade wind regime and the regime of the mid-latitude westerlies. If no storm is superimposed onto this regime as in 1989, wind is rather steady and weak, single events do not stand out, i.e.: No remarkable peaks emerge in the NIWSM time series. NIWSM kurtosis is low. Compared to this scenario, a handful of storms introduce a number of well-defined events to the region, increasing NIWSM kurtosis. NIWSM kurtosis in 1989 and 2010 in subtropical eastern North Atlantic is consistent with these considerations.

3.3.) Southward Displacement of mean NIWSM patterns relative to the Storm Track

Figure 5 suggests that the core storm track residing over Newfoundland and region of high mean-NIWSM in the western subtropical North Atlantic (35 to 45°N, 70 to 30°W, which can be considered to be the NIWSM-equivalent of the core storm track) do not coincide. Rather, the centre of NIWSM activity is shifted approximately 10° to the south of the storm track. Since one would expect NIWSM to be coupled to storms and thus anchored to the storm track, this finding is surprising.

To address this topic, a climatological amplitude spectrum of NCEP/NCAR-wind stress in the western North Atlantic was analysed. The analysing domain enclosed the region 30 to 60°N, 50 to 40°W. Raw spectra of the zonal and meridional wind stress components were calculated for each winter (JFM) running from 1980 to 2013. Squared spectral values of horizontal wind stress were summed up to yield a consistent estimate of wind stress power spectral density. Subsequent zonal averaging was employed for smoothing.

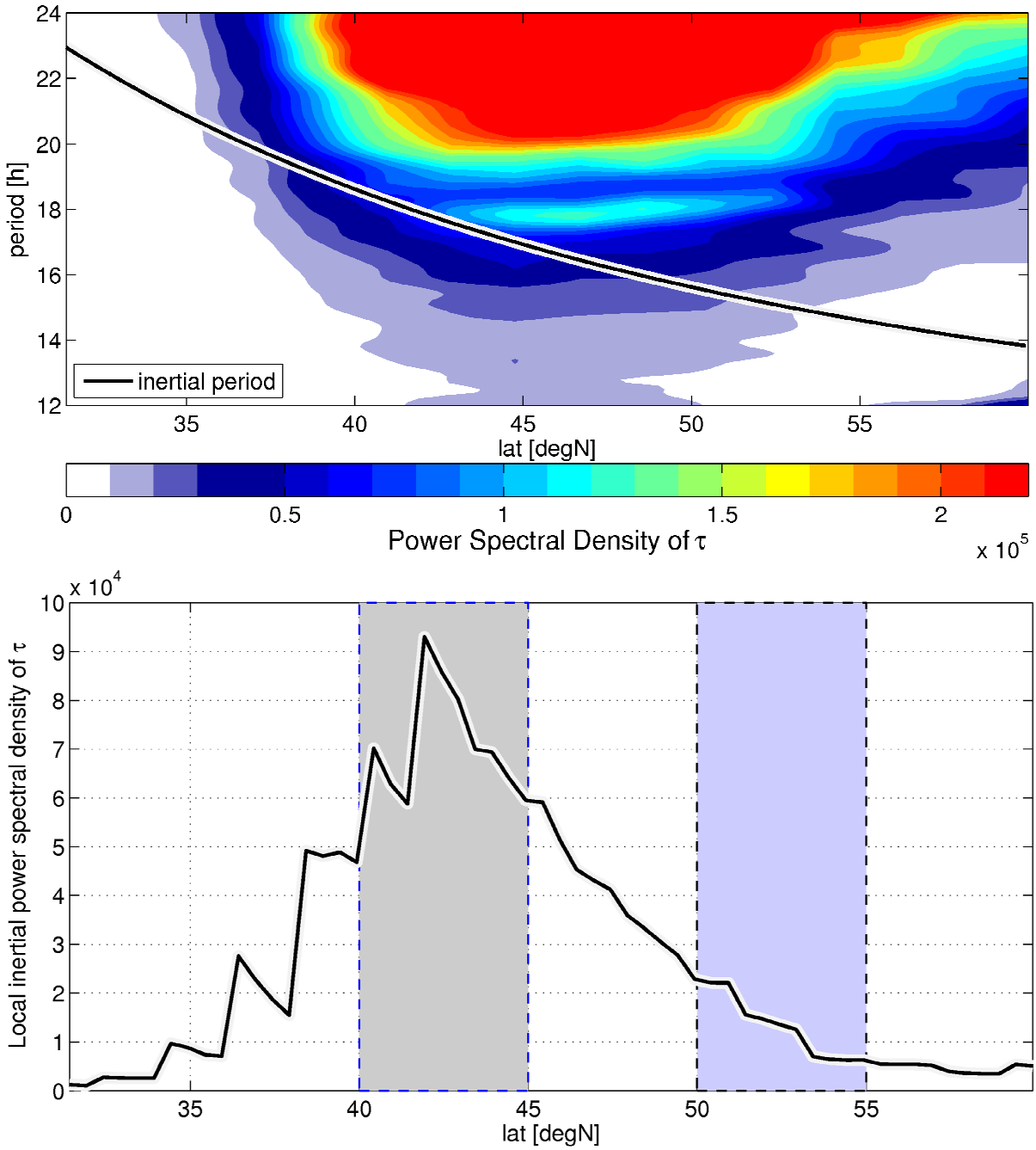

Figure 7: Top: Surface wind stress power spectral density (PSD) in the North Atlantic in dependence on latitude. Amplitude spectra were calculated based on NCEP/NCAR-data (1980 – 2013, 6-hourly samples) for a zonal strip between 50 and 40°W. Raw spectra for the zonal and meridional wind stress component were obtained separately. The summed squares of these components were averaged zonally. The solid line corresponds to the local inertial period. Bottom: "inertial PSD": Power spectral density of surface wind stress corresponding to the inertial frequency in dependence of latitude (cf. black line in top panel). Shaded blue and grey areas correspond to the regions of enhanced mean NIWSM and the North Atlantic climatological storm track, respectively (cf. Figure 5).

Figure 7 (top) shows the resulting distribution of power spectral density in the near-inertial range. It is evident that surface wind stress in subtropical and mid-latitudes exhibits reddish amplitude spectra with cut-off frequencies depending on the latitude: High variability is found in near-inertial periods in a latitude band stretching from 40 to 50°N, with cut-off periods increasing drastically towards the equator and less strongly towards the pole. This is consistent with a similar analysis conducted by Rath et al. (2014) for the Southern Ocean.

However, to explain the offset between mean NIWSM and the storm track, focus has to lie on the near-inertial part of wind stress variability. This part is tied to the variable local Coriolis frequency and does not necessarily pick up the storm track-peak in wind stress variability. Figure 7 (bottom) shows the power spectral density (PSD) of wind stress corresponding to the local inertial frequency ("inertial PSD") in dependence on latitude. It was obtained by following the Coriolis frequency depicted as the black line in the top panel of Figure 7 and charting the corresponding power spectral density on the y-axis. It is evident that the variable inertial frequency decouples variances in the synoptic and near-inertial frequency bands due to the poleward decrease of the local inertial period: The local inertial frequency band does not pick up the storm track-peak in wind stress variability. Rather, the strongest wind stress variability in the near-inertial band occurs to the south of the storm track, because inertial periods are greater in lower latitudes and thus sample the reddish wind stress spectra at lower frequencies. Even if the wind stress spectra were not to vary with latitude, the decreasing Coriolis frequency would result in inertial PSD decreasing with latitude. But since the cut-off frequency is actually varying with latitude and is biggest in the mid-latitudes, inertial PSD is strongest south of the mid-latitudes. Consequently, patterns of mean NIWSM are displaced to the south of the climatological storm track instead of coinciding with it. On an f-plane – i.e. in a world where the Coriolis-parameter is constant – this phenomenon would not occur. Instead, mean NIWSM would be tightly anchored to the storm track.

4.) Model Results

4.1.) Wind Power Input to near-inertial Currents in 1989 and 2010

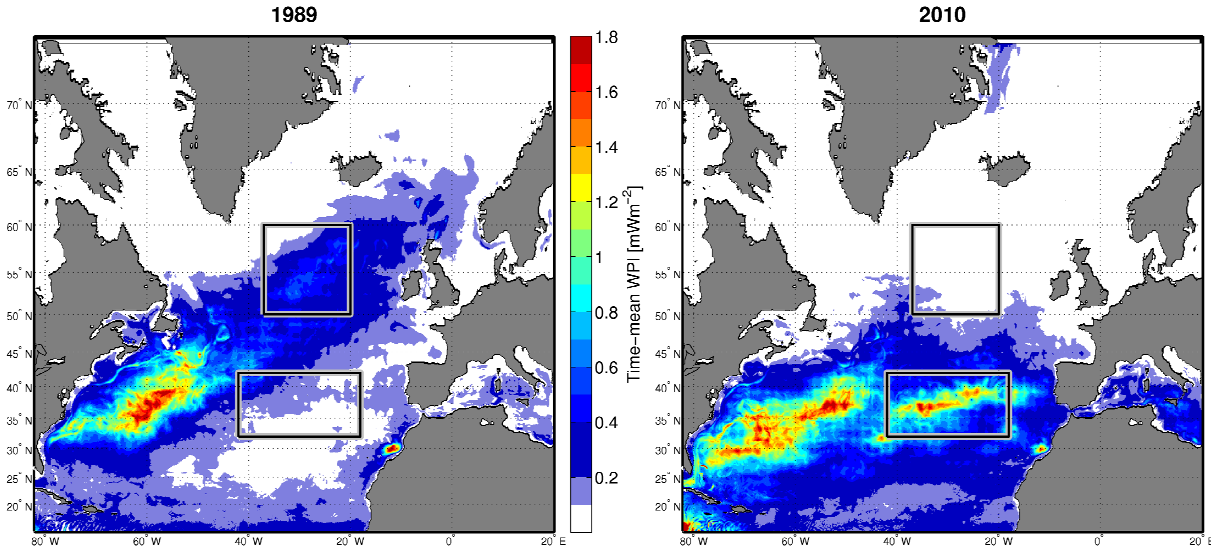

Figure 8: Time-averaged wind power input to surface mixed layer inertial currents in 10^{-3} Wm^{-2} for JFM 1989 (left) and 2010 (right).

The transfer of energy from the atmosphere to the ocean via wind stress and near-inertial currents is crucial to the generation of NIE in the surface mixed layer. Figure 8 shows the spatial distribution of average WPI in response to wind stress forcing for the periods JFM 1989 and 2010, respectively. Magnitudes are comparable for both years, ranging from nearly 0 to 1.7 x 10^{-3} Wm^{-2} (= mWm^{-2}). Considering basin-wide WPI[1], 1989 produced a rate of 6.48 GW compared to 9.64 GW in 2010. This result is surprising because it is counter-intuitive: Since positive NAO phases are associated with increased storminess, and WPI is coupled to wind events, one would assume that 1989 had produced enhanced total WPI instead of 2010.

The 1989 WPI pattern (left) agrees well with the pattern of climatological mean NIWSM (cf. section 3.2., Figure 5): WPI is enhanced to values of up to 1.4 mWm^{-2} in the region 35 to 45°N, 70 to 40°W, with a weak secondary centre occurring to the west of the UK in the central North Atlantic, exhibiting WPI values of roughly 0.5 mWm^{-2}. Note that the secondary centre, albeit weak, matches a region of increased mean NIWSM but is displaced roughly 5° to the south of the positive subpolar storm track anomaly occurring in 1989. (For an explanation of this shift, refer to section 3.3.) Figure 3 also shows a clustering of numerous intense storms in this region. Another interesting feature can be located directly off the African coast at 30°N: WPI shows an extraordinarily strong signal of magnitude 1.7 mWm^{-2} there.

For the pronouncedly negative NAO-conditions of 2010, two regions of enhanced WPI emerge in the subtropical North Atlantic (right panel of Figure 8): The first region roughly corresponds to the one already identified in 1989, although the patch of enhanced WPI is shifted by about 5° to the south and is not as strongly tilted along a southwest-northeasterly axis as in 1989. This region can be regarded as the WPI-equivalent of the core storm track. The second region appears as a zonal strip between 40 and 10°W, stretching towards the coast

[1] The North Atlantic basin in this thesis is considered to be limited to 25 to 65°N, 90°W to 0°E.

of Portugal between 35 and 40°N. The magnitude of WPI in both of these patches reaches values of roughly 1.4 mWm^{-2}. The easterly patch is associated with the shifted and fanned-out storm track shown in Figures 2 (bottom) and 3 (right): As storms travel more frequently towards the Mediterranean basin, they produce high WPI values. North of 50°N, almost no WPI can be identified in 2010. The confined patch of enhanced WPI off the African coast appears unchanged relative to 1989, suggesting that the occurrence of this phenomenon is independent of the NAO phase.

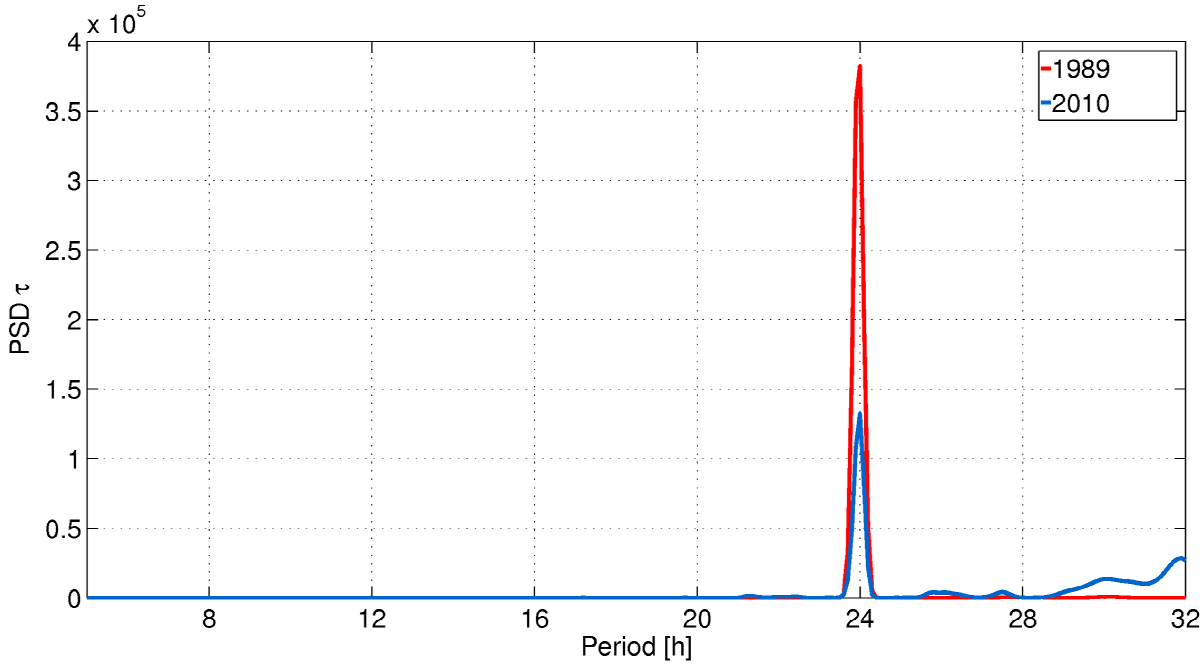

Figure 9: Surface wind stress power spectral density at 29.75°N, 11.75°W (off African coast) for 1989 (red) and 2010 (blue). The PSD was obtained in the same way as in Figure 7.

Indeed, this feature can be associated with the land-sea breeze: At 30°N, the inertial frequency and the diurnal frequency of the land-sea breeze are in resonance and lead to strongly enhanced WPI. To support this hypothesis, Figure 9 shows both the 1989 (red) and 2010 (blue) JFM power spectral density of wind stress at 29.75°N, 11.75°W, which is associated with the location of maximum WPI within the patch of enhanced WPI close to Africa. PSD was calculated in the same fashion as for Figure 7. A pronounced peak emerges at a period of 24 hours, corresponding to both the local inertial period and the period of the land-sea breeze. Note that the peak of the PSD in 1989 is more than twice as large as in 2010. However, no qualitative differences emerge in WPI between the two years. It would be interesting to investigate locations of similar geographical characteristics in other ocean basins.

4.2.) Typical Cases of WPI Events

To illustrate typical single events of WPI – that add up to eventually form seasonally mean WPI – and the associated wind events, Figures 10 and 11 show time series of wind stress and near-inertial surface currents, both in situ and cumulative WPI, cumulative positive and negative contributions to total WPI, and the magnitude of near-inertial currents for a typical situation in the subpolar and subtropical North Atlantic. Reference arrows for the top panel

are of different lengths in the two Figures, but refer to the same magnitude. See Figure caption for details.

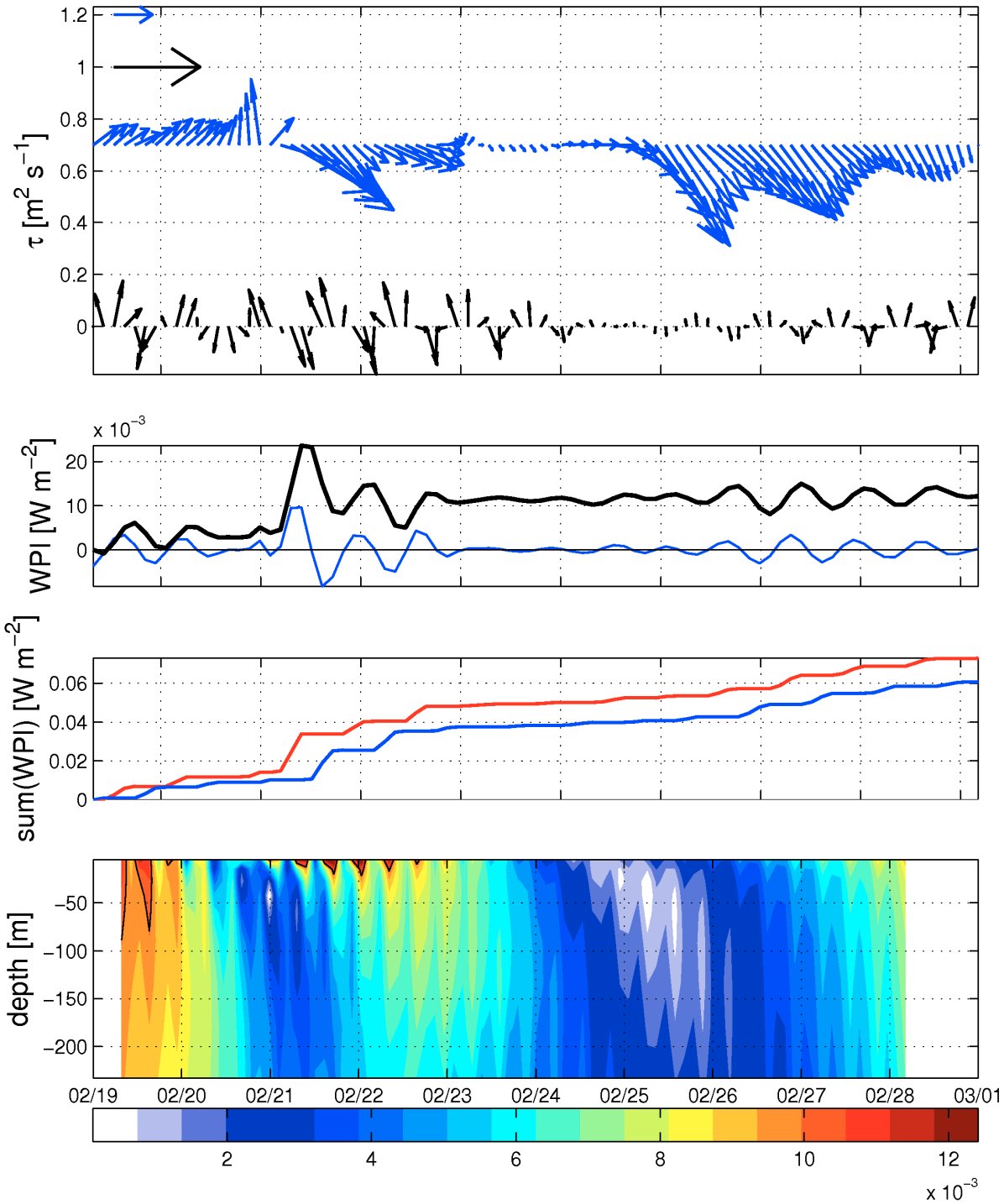

Figure 10: Time series for 52.8°, 26°W (subpolar North Atlantic) in late February obtained from the MITGCM model. Top: Surface wind stress (blue arrows) and near-inertial surface current strength (black arrows). Reference vectors in the top left corner of the panel have lengths of 0.5 m^2s^{-1} and 0.05 ms^{-1} for wind stress and ocean current velocity, respectively. Top middle: WPI (blue) and cumulative WPI (solid black). Bottom middle: Cumulative positive (red) and negative (blue) contributions to total WPI. Bottom: Magnitude of near-inertial currents in ms^{-1}. Black contours are given for the 0.01, 0.015, and 0.02 ms^{-1}-levels.

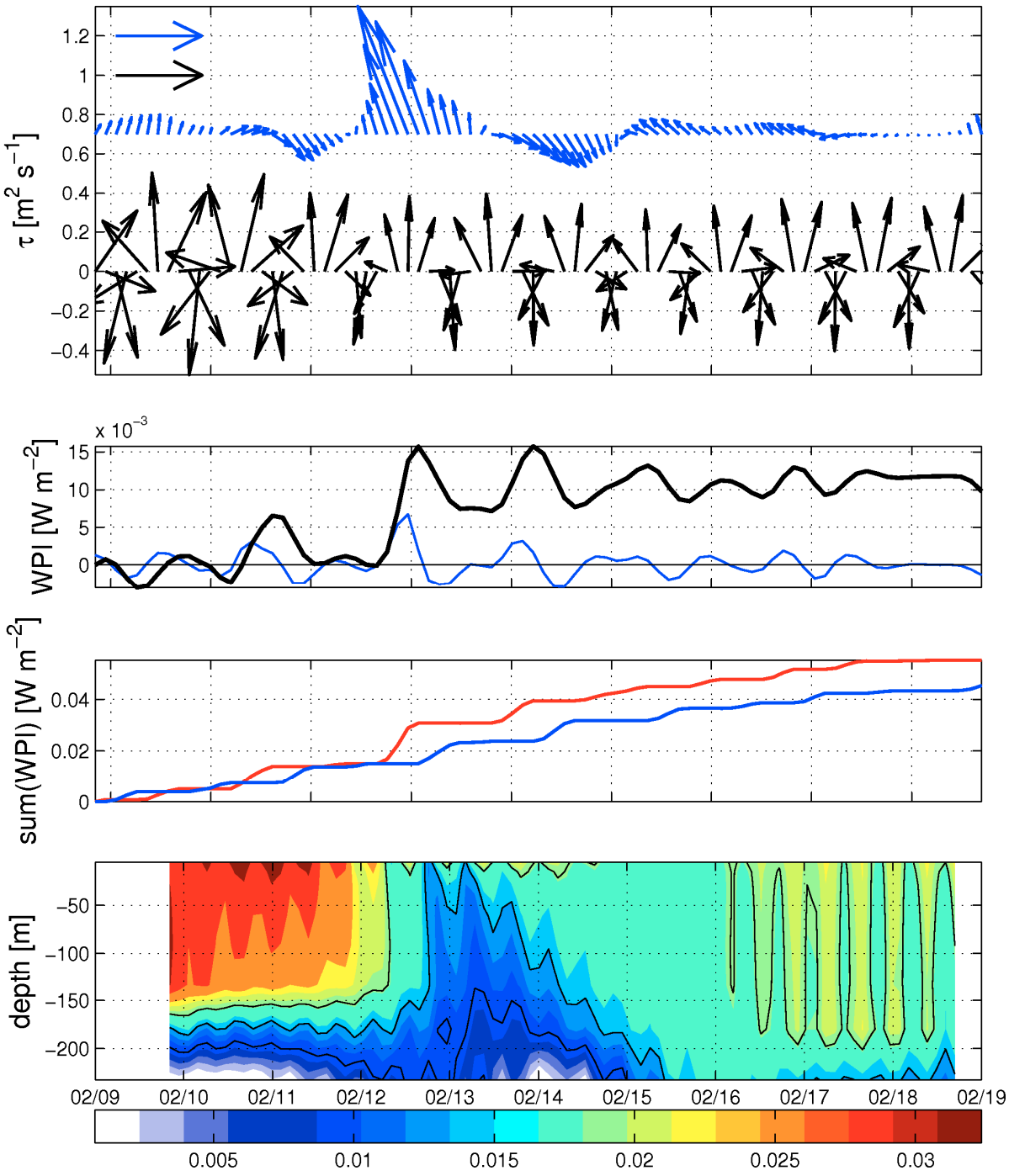

Figure 11: Same as Figure 10, but for 40°N, 27.8°W (subtropical North Atlantic) in mid-February.

In both cases, strong WPI events were triggered by wind events that were characterized by an abrupt change in the direction of and an enhancement of the wind speed. The subsequent WPI event displays the typical oscillatory behaviour associated with the "cancellation effect" (cf. section 4.3.2. for a more detailed explanation): While the near-inertial current rotates below the slower-varying wind stress vector (top panel), the sign of instantaneous WPI changes in accordance with the inertial period (blue line in second panel). Cumulative positive and negative contributions to total WPI (black line, second panel) are sensitive to a number of factors during the wind event, and ultimately set the cancellation ratio of the WPI event (illustration in third panel, more details in section 4.3.2.). Lastly, the wind event might act in two ways on the pre-existing near-inertial currents in the surface layer of the ocean: It

might either induce "fresh" near-inertial currents (this is the case on February 21st in the subpolar ocean, cf. bottom panel of Figure 11) or kill off pre-existing currents before enhancing NIE again (February 13th in the subtropical ocean, Figure 10). In both cases enhanced NIE spreads downwards throughout the mixed layer.

The subpolar case (Figure 10) was taken from 52.8°N, 26°W in late February. A short wind event on February 22nd triggered a positive contribution to WPI, whereas a longer-lived event around February 26th created roughly equal positive and negative contributions that cancelled out in net WPI (thick black line, second panel). Near-inertial oscillations do not exceed currents strengths of 0.015 ms^{-1}. They are observed to spread downwards at a rate of approximately 150 m/day. The mixed layer depth exceeds 250 m.

The subtropical case on the other hand was taken from 40°N, 27.8°W in mid-February. It is shown in Figure 11. A rather short-lived strong wind event sets in at noon on February 12th, meeting a pre-existing near-inertial current. Initial directions of wind speed and inertial oscillation did not coincide, producing negative WPI. On Midnight of February 12th, however, both the strong wind and the inertial current coincided, producing strong positive contributions to WPI. Due to the rather short nature of the wind event relative to the local inertial period, the subsequent negative contribution to WPI was only a fraction of the preceding positive contribution, raising the cumulative WPI from a level of roughly 2.5 mWm^{-2} to 11 mWm^{-2}. Near-inertial currents were rather strong previous to the wind event, exceeding magnitudes of 0.015 ms^{-1}. The onset of the wind event almost erased the inertial current, a weak strengthening and spreading throughout the mixed layer could only be observed beginning on February 14th. The mixed layer has a depth of approximately 200 m.

4.3.) Enhanced subtropical WPI

Returning to seasonally averaged WPI, an interesting feature emerges from comparing absolute mean NIWSM, the storm track, and WPI in 1989 and 2010 (cf. Figures 5, 2, and 8, respectively). Although atmospheric conditions are comparable in the subtropical and subpolar North Atlantic in 2010 and 1989, WPI in the subpolar North Atlantic in 1989 is reduced relative to WPI in the subtropical North Atlantic basin in 2010. To illustrate this point more clearly, Table 1 shows area-averaged mean NIWSM and WPI in both the subtropical and subpolar North Atlantic for 1989 and 2010. The areas of interest are marked as black boxes in Figure 8 and refer to the ocean region that features enhanced WPI in the eastern North Atlantic – i.e. in the region of the storm track tail – either in 1989 or 2010. Mean NIWSM is strongly enhanced both in the subpolar box in 1989 (8.29×10^{-3} Nm^{-2}) and the subtropical box in 2010 (6.10×10^{-3} Nm^{-2}). The ratio of these values is 1.36. For WPI, enhancement occurs in the same boxes for the same years (0.33 mWm^{-2} and 0.54 mWm^{-2} for the subpolar box in 1989 and the subtropical box in 2010, respectively). However, the ratio of subpolar and subtropical WPI is 0.62, indicating that mean NIWSM in the subtropics is much more apt at producing enhanced WPI than it is in the subpolar ocean. What is the reason for this behaviour?

	Latitude	**1989**	**2010**
NIWSM	*Subpolar*	8.29	2.92
[10^{-3} x Nm^{-2}]	*Subtropical*	2.78	6.10
WPI	*Subpolar*	0.33	0.03
[10^{-3} x Wm^{-2}]	*Subtropical*	0.13	0.54

Table 1: Area averages of NIWSM (top) and WPI (bottom) in the subpolar and subtropical box, both for 1989 and 2010. The geographical position and extent of the boxes are shown as black contours in Figure 3 and subsequent maps (Figures 5, 6, 8, 14). The subtropical box encompasses the ocean between 42 and 18°W, 32 and 42°N. The subpolar box encompasses the ocean between 37° and 20°W, 50 and 60°N.

The following subsection investigates WPI in the framework of the simple slab model. Subsection 4.3.2. explains the cancellation effect and lists further processes contributing to enhancing WPI in the subtropical ocean.

4.3.1) Wind Power Input in the Slab Model

Pollard and Millard (1970) introduced the damped slab model to study near-inertial oscillations in the ocean surface mixed layer. It has since been widely used to estimate WPI to near-inertial currents (e.g. D'Asaro, 1985; Alford, 2003). The main assumption of the model is that near-inertial currents are distributed homogeneously throughout the mixed layer instantaneously. Recent research, however, suggests that this assumption is violated for real-world problems and that the slab model should be used cautiously (e.g. Plueddemann and Farrar, 2006; Rath et al., 2014). Indeed, Figures 10 and 11 of this thesis showed that near-inertial currents are surface-arrested at the beginning of a WPI event and only spread throughout the mixed layer subsequently.

Nevertheless, when considering the basic dynamics of a problem involving near-inertial currents, useful results might be obtained. This subsection reviews the basics of the slab model and applies it to a special case that is of relevance for this study.

The slab model equation for the current strength is commonly given in complex notation:

$$\frac{dZ}{dt} + \omega Z = \frac{T}{H}, \tag{1}$$

where $Z = u + iv$ is the complex current strength, $T = (\tau_x + i\tau_y)\ \rho^{-1}$ is the complex wind stress, $\omega = r + if$ is a damping term where f is the Coriolis parameter and r is an artificial damping term that is usually set for 1/r to be 2 to 10 days (D'Asaro, 1985). H is the mixed layer depth. Variations of the mixed layer depth are neglected for simplicity. The general solution to this problem is given by

$$Z(t) = \frac{\int T(t) e^{\omega t} dt + c}{H e^{\omega t}}, \tag{2}$$

with c a constant left to be determined. Note that Z(t) includes both Ekman-driven and near-inertial current components.

Assume that the ocean is at rest initially (t = 0) and consider a meridional wind event of finite length L, i.e.:

$$T(t) = \begin{cases} iT_0 & 0 < t \le L \\ 0 & t > L \end{cases}. \tag{3}$$

Substituting (3) into the full slab model solution (2) yields

$$Z(t) = \begin{cases} \dfrac{iT_0}{\omega H}\left(1 + e^{-\omega t}\right) & 0 < t \le L \\ -\dfrac{iT_0}{\omega H}\left(e^{\omega L} - 1\right)e^{-\omega t} & t > L \end{cases}. \qquad (4)$$

Considering r << f simplifies ω to $\omega \approx if$ and thus (4) becomes

$$Z(t) = \begin{cases} \dfrac{T_0}{fH}\left(1 + e^{-ift}\right) & 0 < t \le L \\ -\dfrac{T_0}{fH}\left(e^{ifL} - 1\right)e^{-ift} & t > L \end{cases} \qquad (5)$$

Note that due to the short nature of the wind event, the resulting currents correspond to near-inertial currents without contributions of Ekman currents. The magnitude of the near-inertial currents is proportional to f^{-1}: Comparable wind forcing excites stronger near-inertial currents at lower latitudes. This is consistent with basic dynamic considerations of inertial oscillations, as are for example provided by Gill (1982).

WPI of such a single event is given by

$$WPI = \mathrm{Re}\left[\int_o^L Z(t)T(t)dt\right] = \underbrace{\frac{T_0^2}{f^2 H}}_{WPI_0}\left(1 - \cos fL\right) = \left(1 - \cos fL\right)\cdot WPI_0 . \qquad (6)$$

Note that the results implied by (6) are of a purely qualitative nature, since the simplifications applied to the slab model and the model itself fail reality in a number of aspects (e.g. specification of the wind event, no pre-existing currents, instantaneous homogenisation of the mixed layer).

In the case of equation (6), the base magnitude WPI_0 of the event is depending on latitude via the factor f^{-2}. Furthermore, the length of the wind event modulates the actual WPI of the event compared to WPI_0. When $fL = n \cdot 2\pi$ and n = 0, 1, 2, …, (i.e. $L = 2\pi n \cdot f^{-1} = nP_I$, where P_I is the inertial period) WPI vanishes. This relationship between the length of a wind event and the modulation of the event's WPI relative to the base WPI allows to define "short" and "long" wind events for the purpose of this thesis. A "*short*" event is a wind event that lasts for roughly half an inertial period. In this case, the base WPI is enhanced due to the cancellation effect. A "*long*" wind event on the other hand lasts for roughly one inertial period[2]. In this case, the event's WPI is decreased relative to the base WPI. However, because the inertial frequency is variable and increases with latitude, a wind event that is considered to be short in the subtropical ocean might be a long wind event in the subpolar ocean. Figure 12 illustrates this effect for a typical subpolar and subtropical case at 30°N and 60°N. The inertial periods at these locations are roughly 24 hours and 14 hours, respectively. Thus, in the subtropical ocean, a wind event lasting for 12 hours is clearly considered short: The cancellation factor (1 – cos *fL*) amounts to roughly 2, enhancement of the base WPI is taking place. The same 12-hour-event in the subpolar ocean, however, results in strong damping of the base WPI. In the framework of this thesis, it can be identified as a long wind event.

[2] Note that since the cancellation factor (1 – cos *fL*) is periodic, the definitions for long and short wind events apply also for integer multiples of themselves.

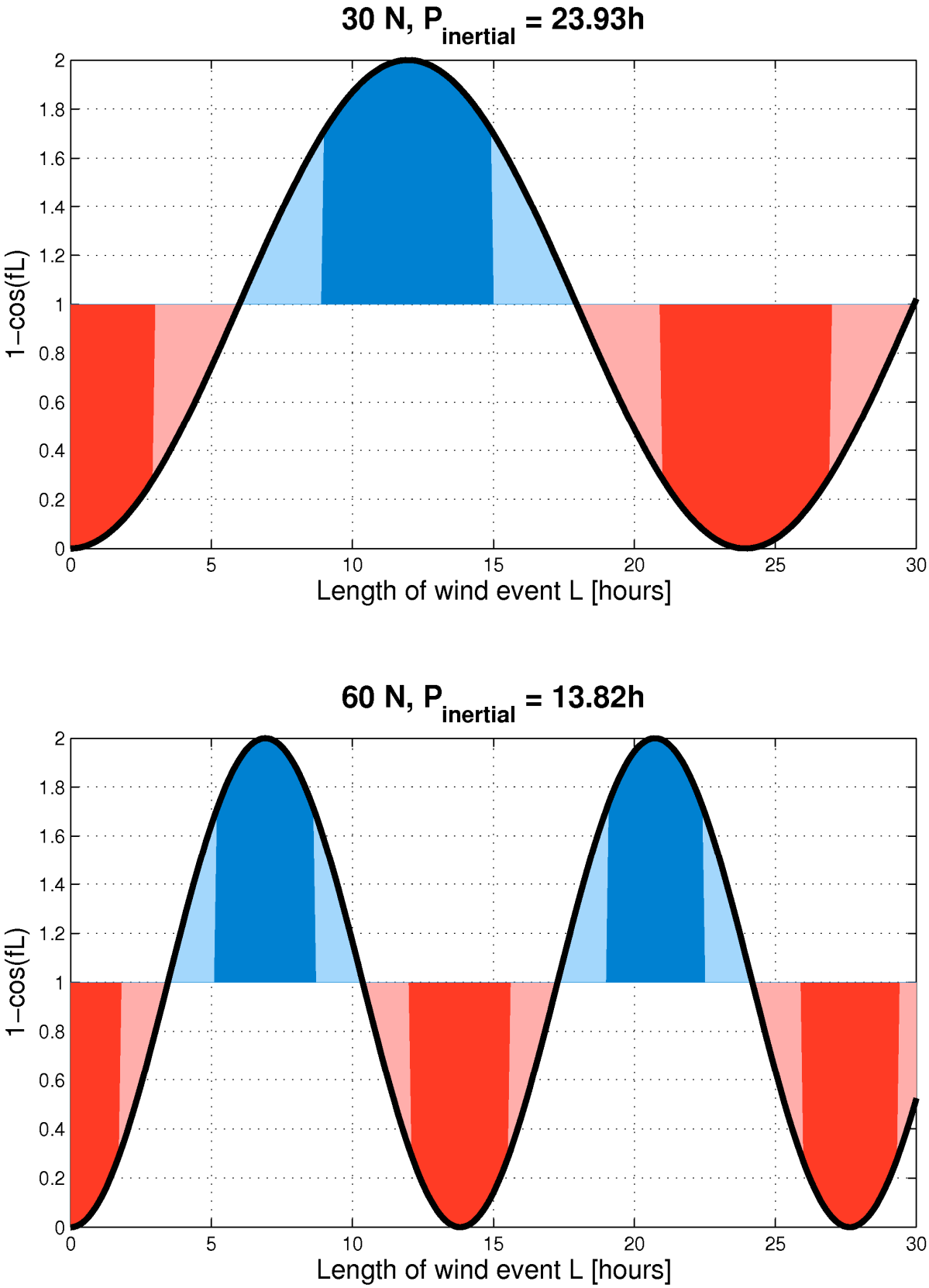

Figure 12: Modulation of "base WPI" (= T_0^2 (f^2 H)$^{-1}$ cf. Equation (6)) due to the length of the wind event as predicted by the slab model. Top: 30°N (subtropical), bottom: 60°N (subpolar). The thick black line and shading denote the amplification factor (1 – cos *fL*), where f is the Coriolis frequency and L the length of the wind event. Red shading denotes damping, blue shading amplification of the base WPI.

4.3.2.) The Cancellation Effect

WPI in this study is calculated as the scalar product of unfiltered wind stress and near-inertial surface currents. Thus, when discussing the preference of WPI for the tropics, both processes having either an effect on the general state of the wind field or on surface inertial currents have to be considered. If either of the two quantities is increased, we expect an increase in the associated WPI as well. This subsection focuses on the effect of the variable Coriolis frequency on the magnitude of inertial oscillations and the cancellation effect. To avoid confusion, we use the following phrases throughout the discussion: *instantaneous* WPI is the scalar product of wind stress and the near-inertial surface current at an arbitrary time step. It is the smallest building block of WPI-related quantities. A time series of WPI shows the evolution of instantaneous WPI with time, which depends on the relative directions of wind stress and the near-inertial current and their respective magnitudes. *Seasonal* WPI is the seasonal average (JFM) of instantaneous WPI at a given location. An *event's* WPI is a summed-up fraction of instantaneous WPI that can clearly be associated with a wind event. According to D'Asaro (1985), it is the top 7% of (instantaneous WPI) samples that provide 50% of the seasonal WPI, i.e.: the strongest events have a great impact on the seasonal average, implying that it is sufficient to consider these strong events when attempting to explain the pattern of seasonal WPI.

Taking the slab model equation (5) and the basic considerations pointed out above as a basis and focussing on the oceanic part of WPI, near-inertial currents are sensitive to both the mixed layer depth and the latitude:

- **Mixed Layer Depth H**: The dependence on the mixer layer depth originates from the slab model and requires the inertial current to be evenly distributed throughout the mixed layer. If this is the case, the near-inertial current strength – and thus, by definition, the near-inertial energy – is inversely proportional to H (Pollard and Millard, 1970). This result should be treated cautiously, since near-inertial currents are both surface-arrested and -intensified initially and take some time to spread through the mixed layer (Rath et al., 2014). Nevertheless, the mixed layer might play a role for long events, and should not be entirely discarded from discussions.
- **Coriolis-parameter f**: Equation (5) points out that the strength of an inertial current is inversely proportional to the Coriolis-parameter, i.e.: It is depending on latitude. This result is consistent with basic theoretical considerations of inertial oscillations (i.e. Gill, 1982). To illustrate this point, Figure 13 shows the average strength of the near-inertial surface currents both for the winters of 1989 and 2010. Near-inertial currents in 1989 have comparable strengths of roughly 0.02 ms^{-1} in the subtropical and subpolar ocean, although wind forcing in the subtropical ocean basin is much weaker (cf. Figures 2, 3, and 5). This suggests that their magnitude is indeed depending on latitude. Another – possibly: minor – factor contributing to the distribution of near-inertial current strengths in 1989 might be the different mixed layer depths in the subtropical and the subpolar ocean. Note that strong similarities with the WPI pattern (Figure 8) in the eastern North Atlantic are evident.

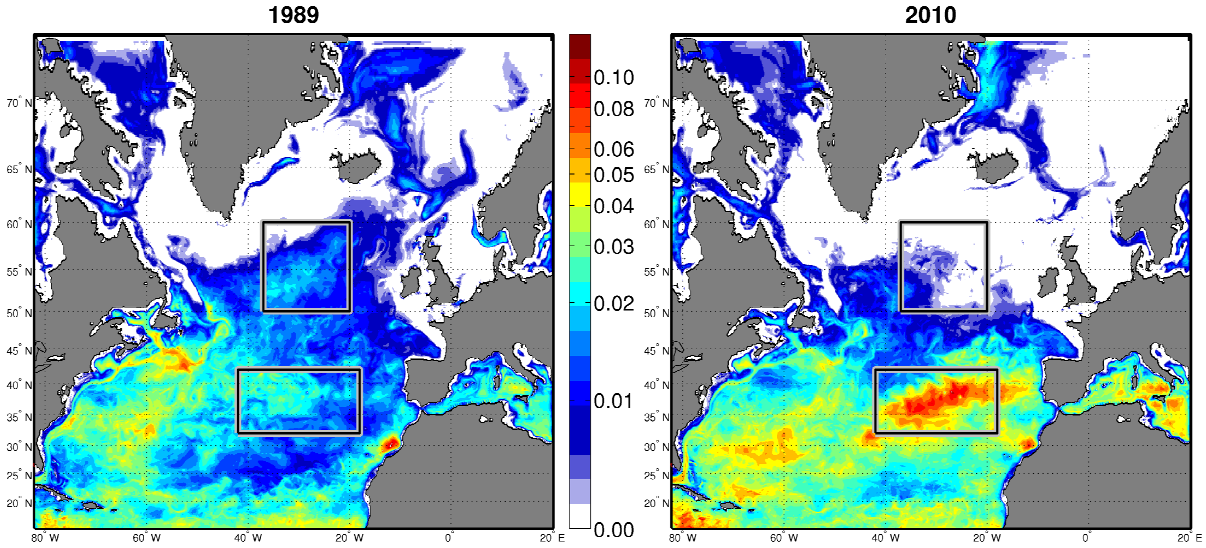

Figure 13: Strength of surface near-inertial currents in 1989 (left) and 2010 (right). "*Surface*" in this case refers to the first layer of the ocean model. The unit is ms^{-1}. Note that the colorbar is logarithmic. Black boxes as in Figure 3.

Apart from modulating the strength of the near-inertial current, the Coriolis parameter also sets the period of the oscillation, with low-latitude near-inertial currents rotating slower than their high-latitude counter parts. This leads to what we call the "*cancellation effect*".

The cancellation effect: Depending on the direction of the wind stress relative to the direction of the near-inertial surface current, instantaneous WPI can be both positive (i.e. wind transfers kinetic energy to the ocean and accelerates near-inertial currents) and negative (wind takes energy out of the ocean and decelerates near-inertial currents). Negative instantaneous WPI occurs if wind stress and the near-inertial current share an anti-parallel component. D'Asaro (1985) argued that in this case shear increases in both the atmospheric and oceanic boundary layers adjoining the air-sea interface. Momentum transfer from the atmosphere to the ocean decreases, because an increased portion of kinetic energy is lost to turbulent dissipation in the boundary layers. The near-inertial current is slowed down.

For an existing near-inertial current, it is very unlikely that the velocity vectors of the wind stress and the ocean currents are locked to each other. Rather, they will diverge at some point, causing the scalar product of wind stress and near-inertial current to vary in time and sign. Typically, the current rotates faster than the wind stress (cf. section 4.2.), causing instantaneous WPI to oscillate at roughly the near-inertial frequency until the wind event abates. This can be seen clearly in Figures 10 and 11.

The oscillatory behaviour of instantaneous WPI is best described for a long wind event that is characterized by relatively constant wind directions. "Long" in this sense refers to events that last for a multiple of roughly one entire inertial oscillation. The ocean current rotates below the influence of the wind stress. Phases of positive (acceleration of the current) and negative (deceleration) scalar products of wind stress and near-inertial current take turns. This means: The event's WPI is the sum of alternating large positive and negative spells of instantaneous WPI. The ratio of these positive and negative contributions depends on the length of the wind event. (Note that in the real world, other factors are of importance as well: How does the direction of the wind change with time? How does the wind speed vary? Is the near-inertial current affected by other oceanic processes, such as advection of NIE? Again: The discussion provided here is of a mainly qualitative nature.) If, for example, the wind event is such that the net-acceleration of the near-inertial current outlasts the net-deceleration, the event's WPI will be enhanced relative to a similar event that lasted half an inertial period

longer or shorter, since positive contributions to the event's WPI are larger than negative contributions. Less cancellation took place. The cancellation effect for this event is favourable for WPI. In the same fashion, it can be unfavourable and even lead to a specific wind event not contributing any net WPI to the seasonal average.

One measure to assess the impact of the cancellation effect is to sum up all positive and negative contributions to WPI during one season and calculate the ratio of the modulus of these sums. This quantity is referred to as "*cancellation ratio*" throughout the thesis. If the cancellation ratio is bigger than 1, total positive contributions to instantaneous WPI exceeded negative WPI, indicating that seasonal WPI is positive.

Inspecting time series of instantaneous WPI at single locations, identifying strong WPI events and charting the associated cancellation ratios (not shown) revealed that the cancellation ratio alone is not a good indicator of whether an event contributes strongly to seasonal WPI or not. Indeed, two types of strong events can be identified: Firstly, short wind events are generally characterized by increased cancellation ratios, i.e. positive WPI contributions outweigh negative WPI contributions. In this case, the event's WPI is relatively large and apt to contribute strongly to seasonal WPI. Secondly, long events lasting for multiple inertial periods usually display low cancellation ratios, since negative and positive contributions are both large and differences producing increased cancellation ratios are small compared to the contributions themselves. Nevertheless, since the magnitude of such a wind event and subsequently the magnitude of the WPI event as well are usually quite large, the small residual between positive and negative contributions adds up with time and amounts to an enhanced event's WPI.

Cancellation ratios themselves are distinctly increased in regions that are rarely struck by strong wind events (not shown), namely in the regions laying in the south of the core storm track (Sargasso Sea in 1989, northern flank of the Caribbean Sea in 2010) and the eastern subtropical Atlantic at about 25°N in 2010. Comparing these patterns with the patterns of individual storm paths (Figure 3) confirms that cancellation ratios are very sensitive to increased intermittency of wind events. This is physically consistent with expectations, since reduced wind activity can be associated with shorter and weaker wind events, imprinting less pronounced inertial oscillations onto the ocean that can easily be "overwritten" by the preceding wind event. Weak pre-existing near-inertial currents in turn benefit the cancellation ratio because the positive contributions to instantaneous WPI at the beginning of a wind event are usually the largest throughout the whole event (cf. Figures 10, 11). This combination – weak and short wind events – explains very well, how the pattern of cancellation ratios is distinctly dominated by regions that are marked by very little wind activity. Unfortunately, these regions are of little interest for the current thesis, since seasonal WPI is bound to be low.

Figure 14 eliminates the bias of the cancellation ratio towards regions with little wind activity. It shows the zonally averaged cancellation ratio in the eastern Atlantic between 40 and 25°W, for 1989 (red) and 2010 (blue). Values range between 1.3 in the subtropics and 1.1 in the subpolar North Atlantic. The cancellation ratio in 2010 is markedly increased in the subtropics relative to 1989. Indeed, little variation is occurring in 1989 with latitude, suggesting that wind events in the 2010 subtropical North Atlantic were more apt in producing increased WPI events due to enhanced cancellation ratios than over the entire ocean in 1989. Note also that the relatively low cancellation ratios in the 1989 subtropics are consistent with previous arguments: Figure 3 confirms that no extratropical cyclone passed the subtropical North Atlantic in the winter of 1989, constraining wind events to be mainly associated with the wind regime of the horse latitudes. The intermittency of wind events thus is relatively low (kurtosis for mean NIWSM < 4.5, cf. Figure 6), consistent with decreased cancellation ratios. Passing storms increase the intermittency of wind events in 2010 (kurtosis ≈ 10), enhancing cancellation ratios.

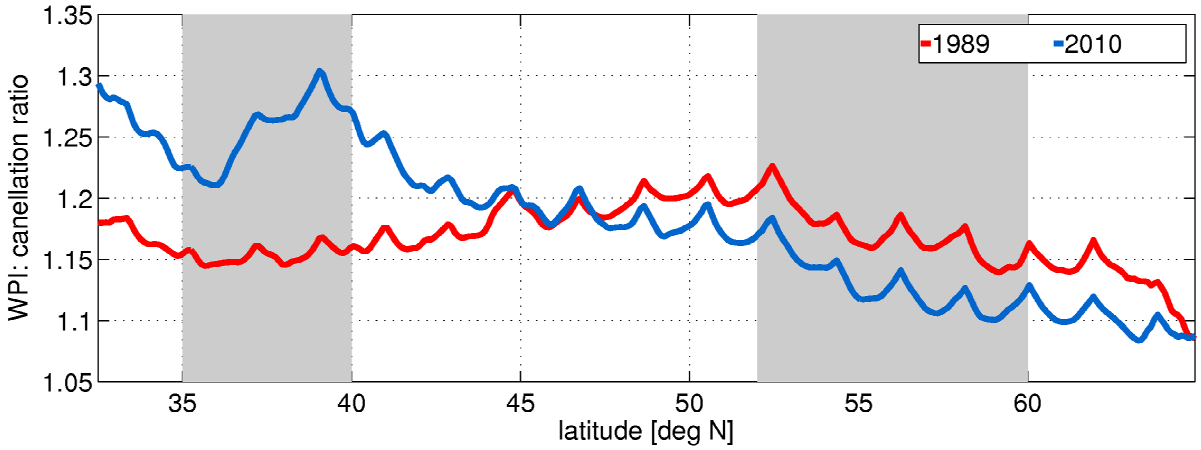

Figure 14: Zonal average of the cancellation ratio (= positive contributions to WPI divided by modulus of negative contributions to WPI). The zonal strip for the analysis is 40 to 10°W.

Overall, we conclude that the cancellation effect measured in terms of the cancellation ratio is strongest in the subtropics, while its impact dwindles with increasing latitude. In our model runs, the cancellation effect abets increased WPI in the 2010 subtropical North Atlantic, but has little effect on seasonal WPI in the subpolar ocean. Next to the latitude-dependence of the near-inertial current strength, it is an important factor in explaining the preference of seasonal WPI for the subtropics.

Note that the cancellation effect described above is qualitatively contained in equation (6): The factor $(1 - \cos fL)$ (cf. Figure 12) describes the enhancement or damping of a base value of WPI depending on the length of the wind event. This is exactly what the physical mechanism associated with the cancellation effect states: Depending on the length of the wind event, cancellation of positive contributions to WPI by negative contributions might be more or less favourable and can result in complete extinction of the event in terms of net contributions to seasonal WPI.

However, the scenario described by the slab model will scarcely apply to the real world in a quantitative sense, due to a number of factors that have been discussed before. Chief among them: Rarely will the ocean be at rest when a wind event sets in. Near-inertial oscillations die off over a time span of roughly 10 days (van Meurs, 1998). Since wind events in the subpolar ocean occur more frequently than this, a wind event will usually be paired up with a pre-existing inertial current. The period of a near-inertial current can be considered to be short compared to synoptic time scales. Thus, a single wind event has roughly a 50%-chance of pairing up with an inertial oscillation that is slowed down initially (instantaneous WPI < 0) instead of being accelerated (WPI > 0)[3]. On the other hand, if a wind event occurs over an ocean populated only by weak or no pre-existing inertial oscillations, the wind stress can not decelerate pre-existing currents but rather induces new inertial oscillations. By default, the initial direction of the newly-created current coincides with the direction of the imposed wind stress and initial WPI is positive. Because storms in the subpolar North Atlantic are more frequent than in the subtropical North Atlantic, pre-existing near-inertial oscillations can be assumed to be more frequent in the subpolar basin, lowering the chance of kick-starting inertial oscillations.

[3] Note that due to the surface confinement of the wind-induced ocean current, a wind event does not have to erase the entire pre-existing inertial oscillation that is well-spread throughout the mixed layer. Rather it will have to eliminate the surface component of the oscillation. This requires considerably less energy and mitigates the effect of pre-existing near-inertial currents to some extent.

Lastly and independently from equation (6), D'Asaro (1985) argues that WPI is enhanced on the southern side of northern hemisphere storms than on the northern side. This effect is due to a number of mechanisms: The cold front, the most efficient weather phenomenon to trigger strong WPI events according to D'Asaro (1985), is usually located on the southern side of a storm. Plus, for a symmetric translating storm such as a hurricane, the wind vector at a fixed location rotates clockwise in time on the southern side of the storm and anti-clockwise on the northern side. The clockwise rotation coincides with the rotational direction of northern hemisphere inertial oscillations and favours WPI (Price, 1981).

Overall, combining all of the above arguments reflects well what is proposed by equation (6): The inverse proportionality to the Coriolis parameter enhances the strength of near-inertial currents in the subtropics. A weak dependence on the mixed layer depth might be present but is not investigated in detail in this study. The magnitude of the wind event naturally increases the event's WPI. From the atmospheric point of view, the length of a wind event acts to amplify or damp the base WPI of the event (i.e. the WPI that could be expected based on the magnitude of the wind event and on the latitude alone). Cancellation effects are more favourable for enhanced seasonal WPI in the subtropics in 2010 than they are in the subpolar ocean in 1989. Further enhancement of seasonal WPI in the tropics can most likely be attributed to features intrinsic to the storms. All of the aforementioned points leave the subtropical ocean basin a region of naturally enhanced WPI.

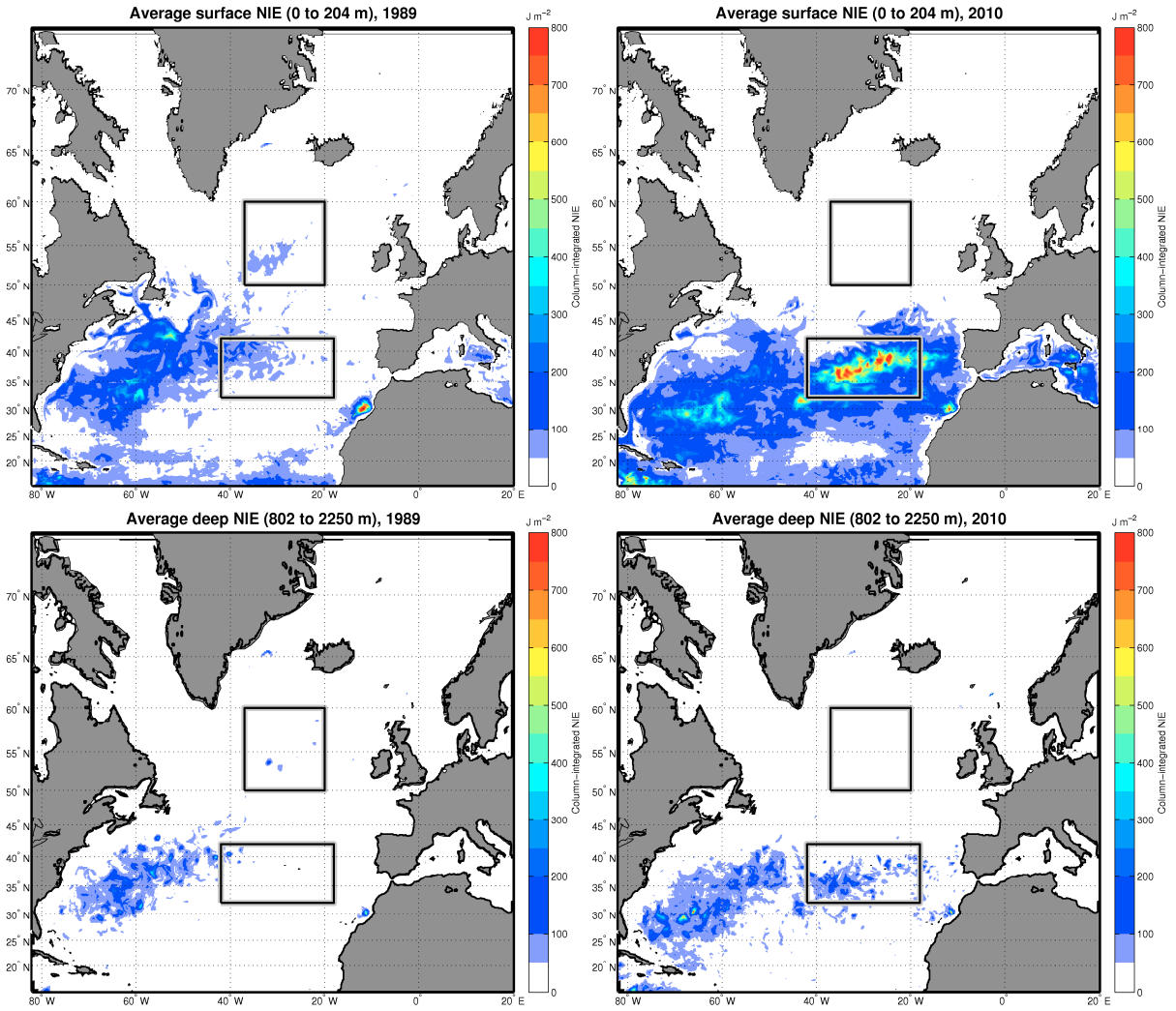

Figure 15: Column-integrated near-inertial energy (NIE). Left: 1989, right: 2010. Top: Surface (0 to 204 m), bottom: deep ocean (802 to 2250 m). Black boxes as in Figure 3.

4.4.) Near-inertial Energy in the deep Ocean

Figure 15 shows column-integrated near inertial energy (NIE) in a surface layer (0 to 204 m, top panels) and a deep layer (802 to 2.250 m, bottom panels). The unit of Jm^{-2} is the same for both sets of Figures. Note, however, that the deep layer is roughly seven times as thick as the surface layer, effectively dwarfing the amount of NIE found on an arbitrary depth level in the deep ocean in comparison to the mixed layer. Furthermore, magnitudes of NIE are usually highly non-linear, with few, small-scale strong events piercing vast regions of low NIE levels.

The structure of the WPI-patterns is well-preserved for both years in the surface layer as well as, to some extent, in the deep layer. Total NIE in the surface layer adds up to 1.02 and 2.08 x 10^{15} J (= PJ) in 1989 and 2010, respectively. Total NIE in the deep layer amounts to 0.39 and 0.62 PJ, respectively. Considering the much bigger thickness of the deep layer (roughly 1.500 m versus 200 m in the surface layer), this result supports what has been found in other studies investigating the export of NIE from the ocean surface into the deep ocean (e. g. Furuichi et al., 2008; Zhai et al., 2009): It is only a fraction of the – mainly – wind-generated surface NIE that escapes into the deep ocean and is potentially available for mixing processes.

In 1989, mixed layer NIE is enhanced to magnitudes of roughly 200 Jm^{-2} in the western subtropical North Atlantic. Single spots of enhanced NIE occur close to the Grand Banks and in an area between 32 and 35°N, 58 and 62°W. This area corresponds to the storm track-equivalent of WPI. The subpolar patch of slightly increased WPI is visible only as a tongue of marginally increased NIE that stretches towards the Nordic Seas. NIE levels do not exceed 100 Jm^{-2} here. The eastern subtropical North Atlantic is basically void of NIE, except for the patch off the African coast at 30°N. The enhanced WPI in this region is effectively transmitted throughout the whole mixed layer. NIE here exceeds 800 Jm^{-2}. The deep layer shows a similar pattern: NIE is enhanced in the western subtropical North Atlantic to a level of roughly 150 Jm^{-2}. The subpolar patch corresponding to enhanced WPI shows up more clearly than it did in the mixed layer case.

In 2010, NIE is visibly enhanced relative to 1989. The western subtropical ocean basin associated with the mean NIWSM and WPI-equivalent of the core storm track shows up with NIE levels of about 450 Jm^{-2}, whereas the subtropical patch of WPI is mirrored much more pronouncedly in mixed layer NIE, producing NIE magnitudes of approximately 700 Jm^{-2}, with peaks exceeding 800 Jm^{-2}. The African patch shows up in a manner comparable to 1989. Although WPI is comparable for the storm track-equivalent and the subtropical region west of Portugal (cf. Figure 8), NIE prefers the eastern subtropical North Atlantic. This result can be linked to the difference in mixed layer depth between the two parts of the ocean basin: Whereas the core storm track region is associated with a naturally deepened mixed layer, the mixed layer in the eastern ocean basin is usually shallow and deepened only little throughout winter. In accordance with previous arguments, this suggests that mixed layer near-inertial currents are enhanced in the eastern subtropical ocean basin relative to the western ocean basin. Hence, surface NIE in the eastern ocean basin can be assumed to be enhanced due to the effect of the mixed layer depth.

The deep layer in 2010 preserves the rough pattern of the surface layer, albeit the dominance of the subtropical patch in the eastern North Atlantic vanishes. Magnitudes of NIE are comparable to 1989, as is the patch of enhanced NIE off the African coast.

5.) Interannual Variability of WPI

Based on the findings of the previous sections and given the fact that running high-resolution models is a rather inefficient way to investigate the variability of WPI, we now establish statistical relationships between WPI and atmospheric quantities as a means of estimating seasonal WPI. In a similar fashion, Rath et al. (2014) found that time-integrated near-inertial wind stress variance (NIWSV) serves as a rather good proxy in the Southern Ocean.

Two possible predictors were chosen to build linear regression models for seasonal WPI: mean NIWSM based on the similarities with WPI patterns, and mean NIWSV based on Rath et al.'s (2014) findings. Both seasonal WPI and the atmospheric quantities have been binned into 5°lon x 5°lat-boxes and area-averaged prior to regression. Motivated by the findings of section 4.3. – i.e. that seasonal WPI prefers the subtropics –, separate regressions have been conducted for different latitude bands. The low latitude band covers latitudes with $\varphi < 35°N$, mid-latitudes: $35°N < \varphi < 50°N$, high latitudes: $50°N < \varphi$. The results of linear regression are shown in Figures 16 and 17 for mean NIWSM and mean NIWSV, respectively. Table 2 summarizes the linear regression models.

	Latitude	**Average WPI [x 10^{-3} Wm^{-2}]**	**RMSE [x 10^{-5} Wm^{-2}]**	**(NRMSE) [%]**	**Slope**
NIWSM	*Low*	4.48	9.63	(8)	0.178
	Mid	4.47	17.71	(14)	0.150
	High	0.94	4.70	(11)	0.037
NIWSV	*Low*		26.48	(21)	12.40
	Mid		29.95	(23)	4.73
	High		10.05	(24)	3.02

Table 2: Overview over linear models for WPI based on mean NIWSM (top) and mean NIWSV (bottom). RMSE and NRMSE were estimated from a leave-one-out cross validation. NRMSE is the normalized RMSE, i.e. RMSE divided by the data range, that is: $WPI_{max} - WPI_{min}$. Latitude ranges for the single model classes were as follows: low: $\varphi < 35°N$, mid: $35°N < \varphi < 50°N$, high: $50°N < \varphi$. Units of the slope parameter are Wm^{-2} / Nm^{-2} and Wm^{-2} / $(Nm^{-2})^2$ for NIWSM and NIWSV, respectively.

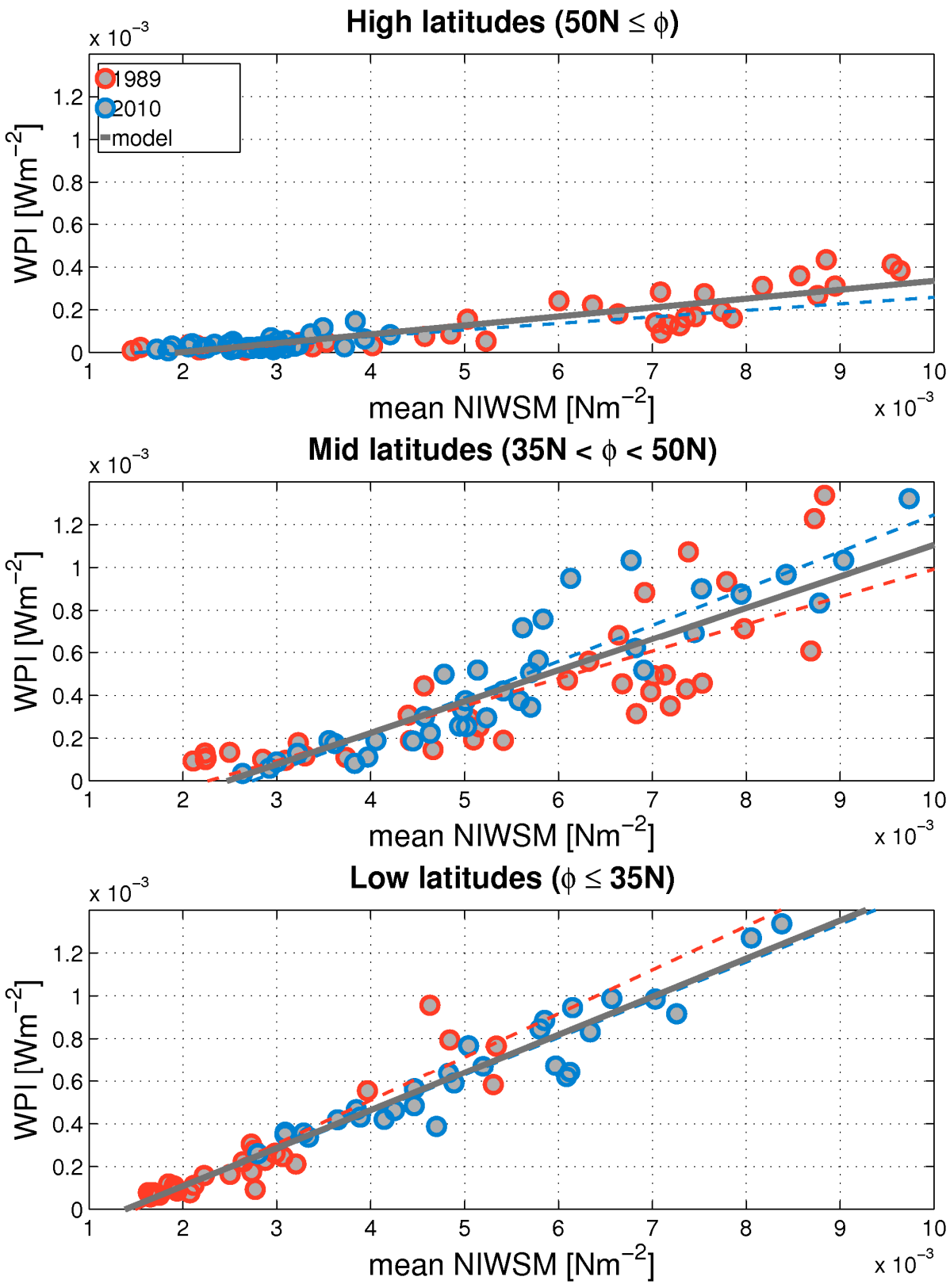

Figure 16: First-order linear regression of WPI on mean NIWSM for high latitudes (top, lat > 50°N), mid-latitudes (middle, 35°N < lat < 50°N) and low latitudes (bottom, lat < 35°N). Mean NIWSM and WPI data have been averaged into 5° lon x 5°lat-bins prior to regression. Red: 1989, blue: 2010. Dashed lines correspond to the linear regression models based on the respective year, solid grey lines to the model derived from both years. The combined model is used for estimating total WPI for 1980 to 2013 (Figure 18).

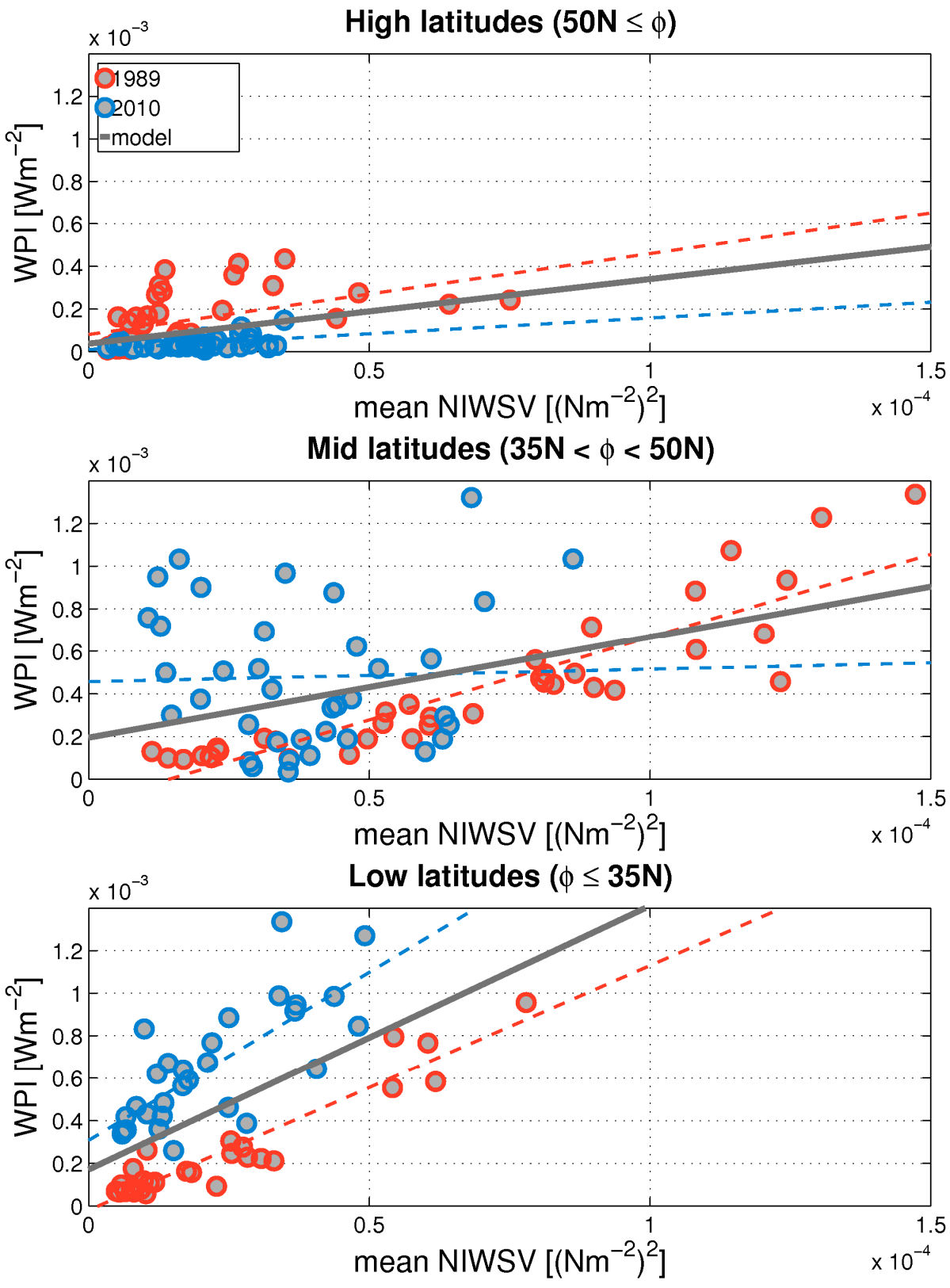

Figure 17: Same as Figure 16, but for mean NIWSV.

For both predictors the slope of the linear regression models decreases drastically towards the poles. This suggests that WPI can indeed be modelled linearly on atmospheric parameters, but that the response of WPI to the atmospheric predictor decreases with latitude, consistent with previous findings. For mean NIWSM, equation (6) suggests that the slope of the model

is both depending on f^{-2} and H^{-1}. For a purely latitudinal effect that is omitting the impact of the variable mixed layer depth, the ratio of the slope of the low-latitude model relative to the high-latitude model would be 2.84. The mean NIWSM-models however exhibit a slope ratio of 4.27, suggesting that additional effects enhance WPI in the subtropics. A discussion of these effects is provided in section 4.3.

Variations in the regression parameters due to the year chosen for regression are small for the mean NIWSM models (Figure 16), but produce considerably divergent predictions for 1989 and 2010 for the mean NIWSV models (Figure 17), resulting in a less promising linear fit of WPI to mean NIWSV when the combined data of 1989 and 2010 is used to develop the linear regression model. However, since the state of the atmosphere can not be expected to be skewed towards either very positive or very negative NAO conditions on the long run, it is the combined model that we choose to estimate past WPI.

A measure of how well a linear regression model is doing in predicting a dependent variable is the (normalized) root-mean-square error ((N)RMSE). The normalized RMSE is the RMSE divided by the range of the predicted variable, i.e. WPI_{max} - WPI_{min} in the case of this study. To estimate the (N)RMSE of our model, we used leave-one-out cross-validation (LOO-CV), which is commonly employed to validate statistical models. For a simple (i.e. non-bootstrapping) version of the LOO-CV, the set of data points for the predictor and the response is split up into a large part that is used for fitting the linear regression model ("*training dataset*") and a small part that is held back for validation ("*testing dataset*"). After building the model from the training dataset, predictions are performed for the testing dataset. These predictions (of the response variable, WPI in our case) are then used to calculate the squared deviations from the response of the testing dataset. To reduce statistical variability, this procedure is repeated for different configurations of the testing dataset. In this study, the testing dataset contained seasonal WPI obtained from the MITGCM model, which was used to validate the estimates of WPI obtained from the linear regression models. We held out each data point of the original dataset once. The single instances of squared deviations from the MITGCM model predictions were then used to calculate the RMSE.

Table 2 shows the RMSE and the NRMSE for each latitude band of our linear regression models for WPI. Values for the mean NIWSM models (roughly 10%) are approximately half as large as values for the mean NIWSV models (roughly 20%) for all latitude bands, suggesting that the models employing mean NIWSM as the predictor are performing considerably better in predicting seasonal WPI.

Based on this finding, we reject mean NIWSV as a suitable atmospheric proxy for WPI and use mean NIWSM to estimate seasonal WPI for each winter (JFM) from 1980 to 2013. Mean NIWSM is binned into the same boxes that were chosen for regression, and regression is applied to each latitude band separately. The area of each grid box is multiplied with the WPI estimate obtained for the respective box, subsequent summation yields the estimates for the entire latitude band. Basin-wide WPI is the sum of WPI in the three latitude bands. The results are shown in Figure 18. Solid lines show the actual estimate for each winter, while dashed lines provide an error estimate (based on the RMSE shown in Table 2). The total error was derived in accordance with the Gaussian rules of the propagation of uncertainty.

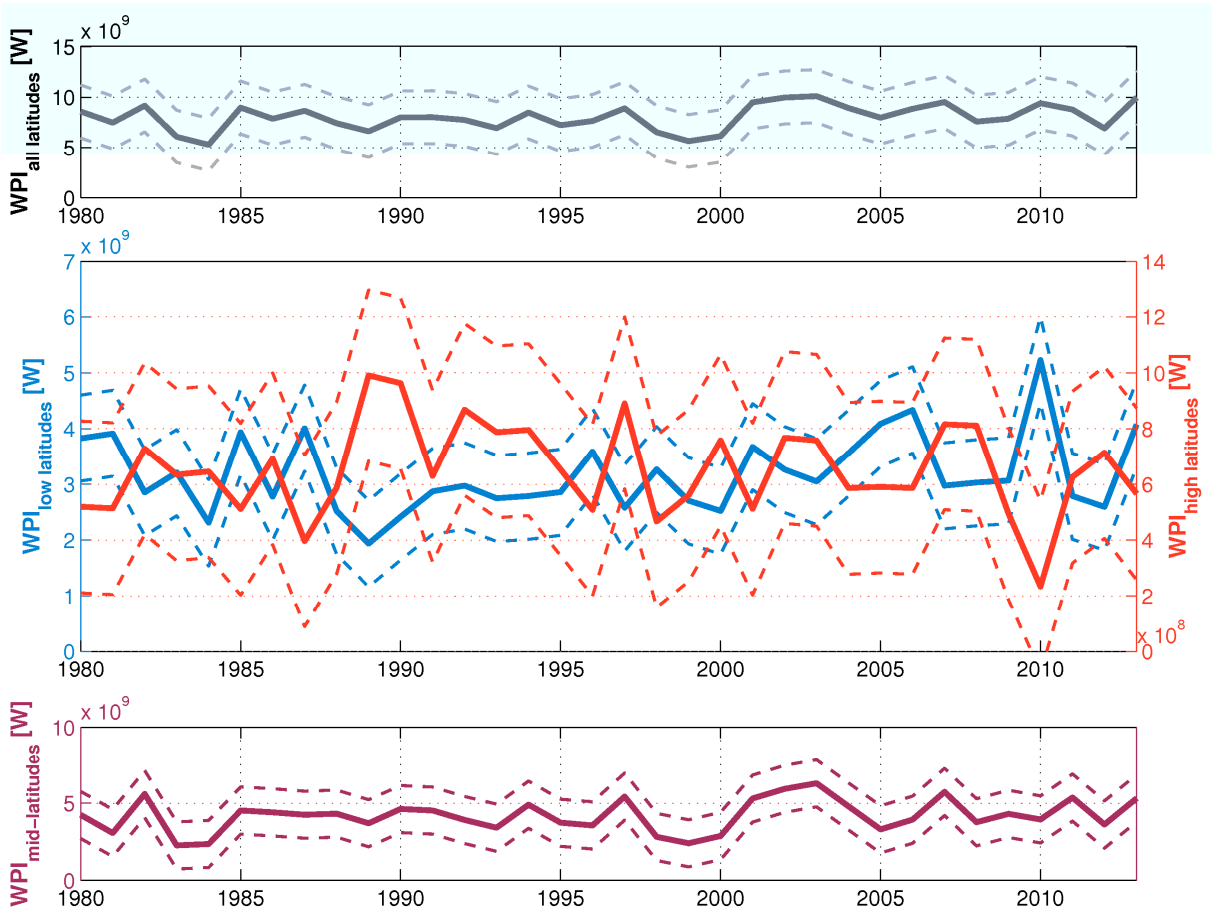

Figure 18: Time series of WPI based on mean NIWSM (linear model: cf. Figure 16). Top: whole basin (= sum of WPI in the three latitude bands shown below), middle: high latitudes (red) and low latitudes (blue), note that the y-axis for these two quantities are not identical, bottom: mid-latitudes. Latitude belts are the same as in Figures 16, 17. Solid lines denote the estimate, dashed lines denote RMSEs that were derived from leave-one-out-cross validation.

	1989		**2010**	
	Model	***Regression***	***Model***	***Regression***
Subpolar	0.98	0.99	0.27	0.23
Mid-latitudes	3.57	3.70	4.30	3.94
Subtropical	1.93	1.94	5.07	5.23
Total	6.48	6.63	9.64	9.40

Table 3: Total WPI (in units of GW) obtained from the MITGCM model ("Model", high resolution), and from the linear regression models ("Regression") (cf. Table 2 for the linear models), both for 1989 and 2010. The rows correspond to different latitude bands. Subpolar: 50°N < φ. Mid-latitudes: 35°N < φ < 50°N. Subtropical: φ < 35°N. The row marked "total" is the sum of the three latitude bands. The entire domain analysed in this context lies between 25 and 65°N, 90°W to 0°E.

Table 3 shows the results of WPI estimated from the linear regression model versus WPI obtained from the MITGCM model for the winters 1989 and 2010. Deviations between the two quantities are small and never exceed 10%[4]. Although this finding is not surprising (since the linear regression models were built with the data from these two years), they confirm our confidence in the approach we have chosen.

[4] Based on the modulus of the difference ($WPI_{MITGCM} - WPI_{regression}$) relative to the MITGCM-model value for the respective latitude band.

Neither total WPI nor WPI for mid-latitudes shows striking features of interannual variability. Correlation coefficients with the NAO time series (cf. Figure 1) are -0.42 and -0.05, respectively. Time series of seasonal WPI in the low and high latitudes on the other hand exhibit interannual variability and are inversely correlated (ρ = -0.75) to each other, suggesting a seesaw-like behaviour: Enhanced subtropical WPI coincides with decreased subpolar WPI and vice versa. Correlation of WPI in these two latitude classes with the NAO is strong as well. Correlation coefficients are -0.87 and 0.81 for low and high latitudes, respectively, supporting the notion that the distribution of WPI is closely related to the configuration of the storm track tail: A shift of the storm track tail pulls the enhanced patch of WPI in the eastern North Atlantic towards the polar ocean basin for positive NAO conditions and pushes it into the subtropics for negative NAO conditions.

Testing the WPI composite averages for significant differences from the 1980 to 2013 climatological mean confirms this hypothesis. We employ Student's *t*-test for unequal sample sizes and equal variances. On the 95% confidence level, WPI composites for positive and negative NAO conditions are significantly different from the climatology for low and high latitudes. Composites for mid-latitudes are not significant. Total WPI differs significantly from the climatology only for negative NAO conditions, but is not significant for positive NAO conditions.

These results support what has already been suggested above: The influence of the NAO on North Atlantic WPI is not as strong as might have been suggested by 2010 and 1989 alone (Figure 8), and becomes manifest mainly in the distribution of WPI, implying that the NAO alters the pattern of WPI but not so much the total rate of WPI across the entire basin. In fact, basin-wide WPI is only weakly related to the NAO, whereas subpolar and subtropical WPI are strongly correlated with the NAO index.

Furthermore, the impact of positive and negative NAO conditions on total WPI is not symmetric: While positive NAO conditions do not lower total WPI significantly below the climatological average, WPI is significantly enhanced during negative NAO conditions. This asymmetry is due to the preference of WPI for the subtropics and the strong relationship between subtropical and subpolar WPI with the NAO. Positive NAO conditions shift the patch of enhanced WPI in the eastern Atlantic towards the subpolar ocean, thus decreasing net WPI in the eastern Atlantic. During negative NAO conditions on the other hand, the storm track tail is shifted towards the subtropics and enhances WPI there. Since mid-latitudinal WPI is essentially uncorrelated with the NAO, it is these eastern Atlantic patches of WPI that determine whether basin-wide WPI is enhanced or not. Because subtropical WPI is exceeding subpolar WPI by roughly an order of magnitude (Figure 18, different y-axis of the middle panel), basin-wide WPI is enhanced for negative NAO conditions but shows no significant signal of decrease during positive NAO conditions.

Overall, the NAO impacts not so much the total rate of WPI to the North Atlantic but rather the pattern of WPI. Because the magnitude of the shifted pattern is not symmetric but enhanced in the subtropics, the response of total WPI is stronger during negative NAO conditions than during positive NAO conditions.

6.) Conclusion

To reveal a possible relationship between the variability of the North Atlantic storm track captured by the NAO-index and spatial characteristics of NIE in the North Atlantic, we used the output of a high-resolution regional ocean model that was forced with NCEP/NCAR wind stress for the months JFM of the years 1989 and 2010. These winters were characterized by exceptionally high (1989) and low (2010) NAO-indices. Total rates of WPI in 1989 and 2010 were 6.48 x 10^9 W (= GW) and 9.64 GW, respectively. Striking differences in the WPI patterns for the two years emerged in the eastern North Atlantic: While a patch of slightly enhanced WPI appears in the subpolar North Atlantic in 1989, WPI is strongly enhanced in the subtropical North Atlantic in 2010. This initially counter-intuitive result can be explained by linking variations in WPI to the variability of the North Atlantic storm track. 1989 produced a storm track that was concentrated in a narrow corridor running into the Nordic Seas past Iceland, whereas the 2010 storm track was more fanned out and allowed storms to travel into the Mediterranean basin in a rather zonal fashion. Analysing patterns of the near-inertial component of wind stress (NIWSM) revealed that marked patterns emerge from the distribution of this quantity in variation with the NAO. However, because the Coriolis frequency decouples synoptic variability and near-inertial variability, the patterns of mean NIWSM are not locked to the storm track but are rather displaced to the south of it. Since NIWSM is the part of the wind stress spectrum that is most efficient in generating WPI, it is appropriate to expect WPI patterns to be shifted relative to the storm track in a similar fashion. Indeed, this is the case.

Positive storm track anomalies are much more efficient in forcing enhanced WPI in the subtropics than they are in the subpolar ocean basin. We identified a number of processes contributing to this behaviour: Due to the Coriolis frequency increasing towards the poles, near-inertial currents are weaker in the subpolar ocean relative to the subtropical ocean, lowering WPI. A weak dependence on the mixed layer depth might be detectable but has not been fully explored within this thesis. Stronger wind stress increases WPI. Furthermore, the cancellation effect states that a given base WPI – i.e. the WPI that can be expected based on the latitude and the strength of the wind event alone – is modulated by the length of the wind event. This effect is favourable for enhanced WPI in the subtropical ocean in 2010, but is of no importance for the subpolar ocean. Other minor atmospheric processes such as features intrinsic to atmospheric storms help to make the subtropical ocean a region of naturally enhanced WPI.

Overall, based on a set of two model simulations representing extreme positive and negative NAO-conditions, we found a strong signal in the spatial pattern of WPI.

These patterns are mirrored in the distribution of NIE within the deep ocean. The magnitude of NIE in the deep ocean is strongly decreased relative to the mixed layer. In 1989, the WPI pattern is translated from the surface into the mixed layer into the deep ocean without many alterations. In 2010, mixed layer NIE mirrors the WPI patterns, albeit NIE is enhanced in the eastern subtropical Atlantic relative to the western part of the basin. We suspect that zonal variations in mixed layer depth are tied to this asymmetric behaviour, allowing stronger near-inertial currents to be created in the eastern subtropical basin. This asymmetry, however, vanishes in the deep ocean.

Lastly, co-analysing patterns of mean NIWSM and the atmospheric storm track reveals a striking similarity between the patterns of mean NIWSM and WPI, suggesting that mean NIWSM might serve as a useful proxy to WPI. We chose mean NIWSM as an atmospheric proxy to WPI over mean NIWSV and built linear models for WPI for three latitude bands. The linear relationship between WPI and mean NIWSM weakens towards the pole,

suggesting that WPI is less sensitive to mean NIWSM in higher latitudes. Using the linear regression models of WPI, we estimated seasonal WPI to the North Atlantic for each winter from 1980 to 2013. Seasonal WPI – i.e. the average rate of WPI in the entire North Atlantic basin – is only weakly correlated with the NAO, as is WPI in mid-latitudes. In low and high latitudes, however, correlation coefficients between the NAO index and WPI exceed magnitudes of 0.8, suggesting that the patterns of WPI in the eastern North Atlantic shift in accordance with the NAO phase. Total WPI is significantly enhanced for negative NAO conditions but is not significantly different from the climatological average for positive NAO conditions. This is due to the fact that WPI prefers the subtropical ocean basin. WPI anomalies in the subpolar ocean basin are very small and thus have a minor influence on total WPI.

The biggest problem in the analysis arises from the employed wind product: NCEP/NCAR wind stress is provided every six hours, which is known to be barely sufficient in high latitudes when it comes to resolving inertial processes. Both inertial variations in wind stress and consequently oceanic inertial oscillations in the North Atlantic might be underestimated. Employing a higher resolved wind data set for future studies is desirable.

Another point arises from the NAO itself. The NAO index during the considered time span (1980 – 2013) is biased towards positive NAO conditions due to multi-decadal variability of the NAO: The mean is 0.5, and composites for positive and negative conditions are 2.4 and -1.3, respectively (cf. Figure 1), suggesting that the sheer magnitude of positive NAO events was stronger than that of negative NAO events. Biases towards the positive NAO phase are likely present in climatological quantities discussed in this thesis as well as in composite quantities. Note, however, that the results of the linear regression models – on the basis of which interannual variability of WPI patterns was discussed – are not subject to the bias. Data for the models was taken from the years 1989 and 2010 exclusively. The NAO indices during these winters were 2.9 and -2.3, respectively, i.e.: They were comparable in magnitude.

Throughout the analysis we emphasized that the physical mechanism tying the NAO to WPI is the variability of the North Atlantic storm track. The storm track on the other hand, albeit intimately related to the NAO (Löptien and Ruprecht, 2005; Greatbatch, 2000), displays co-variability with a set of other patterns of internal climate variability as well, such as the East Atlantic Pattern (Rogers, 1997). In trying to build an index that is capable of capturing the variability of WPI based on storm track variability it could be interesting to include other climate patterns into the analysis, especially the ones that impact the tail of the storm track in the eastern North Atlantic.

Such an index would be a desirable tool to study interannual variability of WPI in the North Atlantic in more depth.

Finally, it would be interesting to trace the surface variability of WPI into the ocean interior in a more detailed fashion and evaluate the spreading of NIE. At this depth, one might tentatively try to estimate the contribution NIE might or might not provide to maintaining the MOC as well as the impact its variability might have on the MOC. Note, however, that Zhai et al. (2009) conducted a study on NIE export into the deep ocean and, via extrapolation of their regional findings, concluded that the amount of NIE available for deep mixing is not exceeding 0.1 TW. Thus, the overall importance of NIE for maintaining the MOC might have been overemphasized. Whether NIE variability has an impact on the MOC remains an open question.

7.) Acknowledgements

Thanks to Richard Greatbatch for supervising my thesis and giving me the opportunity to visit the University of East Anglia in Norwich, UK, for an internship, where I spent quite a productive time working with Xiaoming Zhai (who run the model), laying the groundwork for this thesis. Thanks, Xiaoming, for answering innumerable questions and pointing my work in the right direction in the early stages, as well as participating in eager discussions later on. Thanks, too, to Willi Rath, who put quite an effort into this thesis and helped me mastering some of the trickier technical aspects. I also want to thank Sergey Gulev and Natalia Tilinina of the P. P. Shirshov Institute of Oceanology of the Russian Academy of Sciences for providing the storm path data that helped a lot in interpreting the WPI patterns. Lastly, my thanks go out to the incredibly supportive and patient IT staff of the UEA and the High Performance Cluster of the UEA, which hosted my programming work, as well as to Eva Nowatzki for patiently spell-checking the thesis.

8.) Bibliography

Alford, M. H. (2003). Improved global maps and 54-year history of wind-work on ocean inertial motions. *Geophysical Research Letters*, *30*(8), 1424. doi:10.1029/2002GL016614

Anderson, D. L. T., & Gill, A. E. (1979). Beta Dispersion of Inertial Waves. *Journal of Geophysical Research*, *84*(2).

Benedict, J. J., Lee, S., & Feldstein, S. B. (2004). Synoptic View of the North Atlantic Oscillation. *Journal of the Atmospheric Sciences*, *61*(2), 121–144. Retrieved from http://journals.ametsoc.org/doi/abs/10.1175/1520-0469(2004)061<0121:SVOTNA>2.0.CO;2

D'Asaro, E. A. (1985). The Energy Flux from the Wind to Near-Inertial Motions in the Surface Mixed Layer. *Journal of Physical Oceanography*, *15*, 1043–1059.

Furuichi, N., Hibiya, T., & Niwa, Y. (2008). Model-predicted distribution of wind-induced internal wave energy in the world's oceans. *Journal of Geophysical Research: Oceans*, *113*(C9), C09034. doi:10.1029/2008JC004768

Gill, A. E. (1982). *Atmsophere-Ocean Dynamics* (p. 662). Academic Press.

Gill, A. E. (1984). On the Behaviour of Internal Waves in the Wakes of Storms. *Journal of Physical Oceanography*, *14*, 1129–1150.

Greatbatch, R. J. (2000). The North Atlantic Oscillation. *Stochastic Environmental Research and Risk Assessment*, *14*(4), 0213–0242. Retrieved from http://www.springerlink.com/index/10.1007/s004770000047

Gulev, S. K., Zolina, O., & Grigoriev, S. (2001). Extratropical cyclone variability in the Northern Hemisphere winter from the NCEP / NCAR reanalysis data. *Climate Dynamics*, *17*, 795–809.

Hurrell, J. W. (1995). Decadal trends in the north atlantic oscillation: regional temperatures and precipitation. *Science*, *269*, 676–679. Retrieved from http://www.ncbi.nlm.nih.gov/pubmed/17758812

Hurrell, J. W., Kushnir, Y., & Visbeck, M. (2001). The North Atlantic Oscillation. *Science*, *291*(January), 603–604.

Jochum, M., Briegleb, B. P., Danabasoglu, G., Large, W. G., Norton, N. J., Jayne, S. R., … Bryan, F. O. (2013). The Impact of Oceanic Near-Inertial Waves on Climate. *Journal of Climate*, *26*(9), 2833–2844. doi:10.1175/JCLI-D-12-00181.1

Kalnay, E., Kanamitsu, M., Kistler, R., Collins, W., Deaven, D., Gandin, L., … Joseph, D. (1996). The NCEP/NCAR 40-year reanalysis project. *Bulletin of the American Meteorological Society*, *77*(3), 437–471. doi:10.1175/1520-0477(1996)077<0437:TNYRP>2.0.CO;2

Kunze, E. (1985). Near-Inertial Wave Propagation in Geostrophic Shear. *Journal of Physical Oceanography*, *15*, 544–565.

Lau, N.-C. (1988). Variability of the Observed Midlatitude Storm Tracks in Relation to Low-Frequency Changes in the Circulation Pattern. *Journal of the Atmospheric Sciences*, *45*(19), 2718–2743.

Löptien, U., & Ruprecht, E. (2005). Effect of Synoptic Systems on the Variability of the North Atlantic Oscillation. *Monthly Weather Review*, *133*(10), 2894–2904. Retrieved from http://journals.ametsoc.org/doi/abs/10.1175/MWR3007.1

Marshall, J., Kushnir, Y., Battisti, D., Chang, P., Czaja, A., Dickson, R., … Visbeck, M. (2001). North Atlantic Climate Variability: Phenomena, Impacts and Mechanims. *International Journal of Climatology*, *21*, 1863–1898.

Munk, W., & Wunsch, C. (1998). Abyssal recipes II: energetics of tidal and wind mixing. *Deep Sea Research Part I Oceanographic Research Papers*, *45*(12), 1977–2010. Retrieved from http://linkinghub.elsevier.com/retrieve/pii/S0967063798000703

Oort, A. H., Anderson, L. A., & Peixoto, J. P. (1994). Estimates of the energy cycle of the oceans. *Journal of Geophysical Research: Oceans*, *99*(C4), 7665–7688. doi:10.1029/93JC03556

Plueddemann, A. J., & Farrar, J. T. (2006). Observations and models of the energy flux from the wind to mixed-layer inertial currents. *Deep Sea Research Part II: Topical Studies in Oceanography*, *53*, 5–30. doi:10.1016/j.dsr2.2005.10.017

Pollard, R. T., & Millard, R. C. J. (1970). Comparison between observed and simulated wind-generated inertial oscillations. *Deep Sea Research and Oceanographic Abstracts*, *17*(4), 153–175. doi:http://dx.doi.org/10.1016/0011-7471(70)90043-4

Price, J. F. (1981). Upper Ocean Response to a Hurricane. *Journal of Physical Oceanography*, *11*(2), 153–175. doi:10.1175/1520-0485(1981)011<0153:UORTAH>2.0.CO;2

Rath, W. (2013). *The influence of ocean-surface-velocity-dependent wind stress on the dynamics of the Southern Ocean: The near-inertial and the sub-inertial response*. Christian-Albrechts-Universität Kiel. Retrieved from http://oceanrep.geomar.de/22949/

Rath, W., Greatbatch, R. J., & Zhai, X. (2013). Reduction of near-inertial energy through the dependence of wind stress on the ocean-surface velocity. *Journal of Geophysical Research: Oceans*, *118*(6), 2761–2773. doi:10.1002/jgrc.20198

Rath, W., Greatbatch, R. J., & Zhai, X. (2014). On the spatial and temporal distribution of near-inertial energy in the Southern Ocean. *Journal of Geophysical Research: Oceans*, *119*(1), 359–376. doi:10.1002/2013JC009246

Rogers, J. C. (1997). North Atlantic Storm Track Variability and its Association to the North Atlantic Oscillation and Climate Variability of Northern Europe. *Journal of Climate*, *10*, 1635–1647.

Thomson, R. E. (1983). A comparison between computed and measured oceanic winds near the British Columbia coast. *Journal of Geophysical Research: Oceans*, *88*(C4), 2675–2683. doi:10.1029/JC088iC04p02675

Ulbrich, U., Leckebusch, G. C., & Pinto, J. G. (2009). Extra-tropical cyclones in the present and future climate: A review. *Theoretical and Applied Climatology*, *96*(1-2), 117–131. doi:10.1007/s00704-008-0083-8

Van Meurs, P. (1998). Interactions between Near-Inertial Mixed Layer Currents and the Mesoscale: The Importance of Spatial Variabilities in the Vorticity Field*. *Journal of Physical Oceanography*, *28*, 1363–1388.

Watanabe, M., & Hibiya, T. (2002). Global estimates of the wind-induced energy flux to inertial motions in the surface mixed layer, *29*(8), 2–5.

Wunsch, C. (1998). The Work Done by the Wind on the Oceanic General Circulation. *Journal of Physical Oceanography*, *28*(11), 2332–2340. doi:10.1175/1520-0485(1998)028<2332:TWDBTW>2.0.CO;2

Zhai, X., Greatbatch, R. J., Eden, C., & Hibiya, T. (2009). On the Loss of Wind-Induced Near-Inertial Energy to Turbulent Mixing in the Upper Ocean. *Journal of Physical Oceanography*, *39*(11), 3040–3045. doi:10.1175/2009JPO4259.1

Zhai, X., & Marshall, D. P. (2012). Vertical Eddy Energy Fluxes in the North Atlantic Subtropical and Subpolar Gyres. *Journal of Physical Oceanography*, *43*(1), 95–103. doi:10.1175/JPO-D-12-021.1

ERKLÄRUNG

Hiermit erkläre ich, dass ich die vorliegende Arbeit selbständig und ohne fremde Hilfe angefertigt und keine anderen als die angegebenen Quellen und Hilfsmittel verwendet habe. Die eingereichte schriftliche Fassung der Arbeit entspricht der auf dem elektronischen Speichermedium.
(Name der Datei: Dippe_903123_MSc_Thesis)

Weiterhin versichere ich, dass diese Arbeit noch nicht als Abschlussarbeit an anderer Stelle vorgelegen hat.

_____

Datum, Unterschrift